Hydrology of a Perennial Firn Aquifer in Southeast Greenland: An Overview Driven by Field Data

Olivia Miller[1] , D. Kip Solomon[1] , Clément Miège[2] , Lora Koenig[3] , Richard Forster[4] , Nicholas Schmerr[5] , Stefan R. M. Ligtenberg[6] , Anatoly Legchenko[7] , Clifford I. Voss[8] , Lynn Montgomery[9] , and Joseph R. McConnell[10]

[1]Department of Geology and Geophysics, University of Utah, Salt Lake City, UT, USA, [2]Department of Geography, Rutgers, The State University of New Jersey, New Brunswick, NJ, USA, [3]National Snow and Ice Data Center, University of Colorado Boulder, Boulder, CO, USA, [4]Geography Department, University of Utah, Salt Lake City, UT, USA, [5]Department of Geology, University of Maryland, College Park, MD, USA, [6]Institute for Marine and Atmospheric research Utrecht (IMAU), Utrecht University, Utrecht, Netherlands, [7]Institute for Geosciences and Environmental Research and Research Institute for Development, University of Grenoble, Grenoble, France, [8]U.S. Geological Survey, Menlo Park, CA, USA, [9]Atmospheric and Oceanic Science Department, University of Colorado Boulder, Boulder, CO, USA, [10]Division of Hydrologic Sciences, Desert Research Institute, Reno, NV, USA

Abstract Firn aquifers have been discovered across regions of the Greenland ice sheet with high snow accumulation and melt rates, but the processes and rates that sustain these aquifers have not been fully quantified or supported by field data. A quantitative description of the hydrology of a firn aquifer upslope from Helheim Glacier that integrates field measurements is presented to constrain melt and recharge rates and timing, temporal variations in temperature and water levels, and liquid-water residence time. Field measurements include weather data, firn temperatures, water levels, geochemical tracers, and airborne radar data. Field measurements show that once the firn column is temperate (0°C), meltwater from the surface infiltrates to the water table in less than 2 days and raises the water table. Average recharge is 22 cm/year (lower 95% confidence interval is 13 cm/year and upper 95% confidence interval is 33 cm/year). Meltwater within the recently formed aquifer, which flows laterally downslope and likely discharges into crevasses, has a mean residence time of ~6.5 years. Airborne radar data suggest that the aquifer in the study area continues to expand inland, presumably from Arctic warming. These comprehensive field measurements and integrated description of aquifer hydrology provide a comprehensive, quantitative framework for modeling fluid flow through firn, and understanding existing and yet undiscovered firn aquifers, and may help researchers evaluate the role of firn aquifers in climate change impacts.

1. Introduction

Firn is snow older than 1 year transitioning to ice from densification. Firn contains substantial pore space that can become saturated and store or transmit meltwater. Firn aquifers form when sufficient surface melt-water infiltrates to depth, warming the subsurface firn to the melting point, such that additional meltwater can fully saturate firn and persist perennially in the liquid phase. Large perennial firn aquifers located around the perimeter of the Greenland ice sheet have recently been discovered (Forster et al., 2014; Miège et al., 2016) and could contribute up to 0.4 mm of sea level rise if they drained completely (Koenig et al., 2014). These perennial firn aquifers store meltwater within the compacting saturated snow/firn pore space throughout the year and persist over multiple years (Miège et al., 2016). Although seasonal to perennial firn aquifers have been observed in smaller mountain glaciers (generally temperate) in select locations around the world (Fountain, 1989; Kawashima, 1997; Oerter & Moser, 1982; Schneider, 1999; Sharp, 1951; Vallon et al., 1976), the aquifers within the Greenland ice sheet represent a much larger and flatter reservoir for storing and transmitting liquid water within the ice sheet on decadal time scales. In Greenland, aquifers form within the percolation zone at elevations between 1,200 and 2,000 m, in areas of high snow accumulation and melt rates (Forster et al., 2014; Kuipers Munneke et al., 2014; Miège et al., 2016). The high snow accumulation provides sufficient insulation and pore space at depth to retain meltwater (Kuipers Munneke et al., 2014).

Firn in Greenland has the potential to store considerable volumes of meltwater (300 to 1,300 Gt) and to serve as a buffer against sea level rise (Harper et al., 2012). Retention and refreezing of meltwater prevents ~40% to 46% of rain and meltwater from reaching the ocean (Steger et al., 2017; van Angelen et al., 2012, 2013). However, pore space volume is predicted to decrease by over 50% by the end of the 21st century as refrozen meltwater fills firn pore space, thereby decreasing firn storage capacity and accelerating future surface mass loss (Machguth et al., 2016; Pfeffer et al., 1991; van Angelen et al., 2013).

In contrast to areas where meltwater refreezes (and contributes to long-term storage), most meltwater in the firn aquifer does not refreeze or contribute to storage. Although initially thought to store meltwater for longer periods and therefore delay runoff, flow measurements have shown that water flows through and discharges from the aquifer relatively quickly (mean specific discharge of 4.3×10^{-6} m/s) (Miller et al., 2018). This suggests that aquifers do not buffer sea level rise as they do not contribute to long-term meltwater storage. Meltwater movement through aquifers thus has implications for ice sheet mass balance estimates, which are dominated by surface mass-balance processes over ice discharge (e.g., Enderlin et al., 2014). This underscores the need to characterize the hydrology, as it relates to surface mass balance processes, of firn aquifers in Greenland.

The conceptual overview presented here includes a unique data set and conceptual description of firn aquifer hydrology. This paper presents the first measurements of firn aquifer temperature profiles and water levels throughout the year, aquifer recharge amounts and timing, firn and liquid water age, timing of aquifer formation, and monitoring of aquifer expansion beyond 2014. In addition to environmental tracer and radar methods to constrain aquifer formation timing, a new method using salt mass balance is introduced. These measurements are integrated with prior measurements of the aquifer geometry and hydraulic properties to characterize the hydrology of the firn aquifer.

It is expected that as the climate warms, firn aquifer area and occurrence will increase and expand as melt area and amount increase. This expansion may include new locations such as Antarctica and other glaciers around the world becoming temperate, in addition to areas without aquifers in Greenland. As a newly discovered and extensive component of the ice sheet hydrology and surface mass balance, firn aquifers that ultimately discharge to the ocean are anticipated to become increasingly important in quantifying and predicting ice sheet mass balance and sea level rise. Results from this study could serve the numerical modeling community to test and improve firn models and better simulate meltwater flow and retention in firn for further constraining ice sheet mass balance, runoff, and subsequent sea level rise.

2. Methods

2.1. Site Description

The study area is located in the southeast region of the Greenland ice sheet, upslope of Helheim Glacier, ~60 km west of Sermilik Fjord, between ~1,500 and 1,700 m above sea level (Figure 1). The area is characterized by high precipitation and melt rates (Forster et al., 2014; Kuipers Munneke et al., 2014; Miège et al., 2013).

Prior in situ and remote geophysical work at Helheim firn aquifer has defined some of its basic characteristics. The water table depth, elevation, and extent were determined by ground-penetrating radar and water level measurements, while the base of the aquifer was determined by active source seismic surveys and borehole dilution tests (Miège et al., 2016; Miller et al., 2018; Montgomery et al., 2017). On average, the water table at Helheim firn aquifer is located at 16.0 ± 5 m depth, and the base of the aquifer (where all water in pore space is frozen) is located at ~27.5 $\pm$ 4 m depth, resulting in an average thickness of ~11.5 m (Miège et al., 2016; Montgomery et al., 2017). The aquifer stores an average of 760 kg/m^2 liquid water (Legchenko et al., 2018a, 2018b; Montgomery et al., 2017). Hydraulic conductivity profiles were measured with depth-specific slug tests and as a depth-integrated measurement with aquifer tests (Miller et al., 2017). Water flow within the aquifer also was quantified and found to follow Darcy's law (Miller et al., 2018). This location has a history of measurements including annual measurements from the NASA Operation IceBridge (OIB) airborne campaign starting in the spring of 2010 (Miège et al., 2016) and radar data collected by the Center for Remote Sensing of Ice Sheet (CReSIS, 2017., http://ftp.data.cresis.ku.edu).
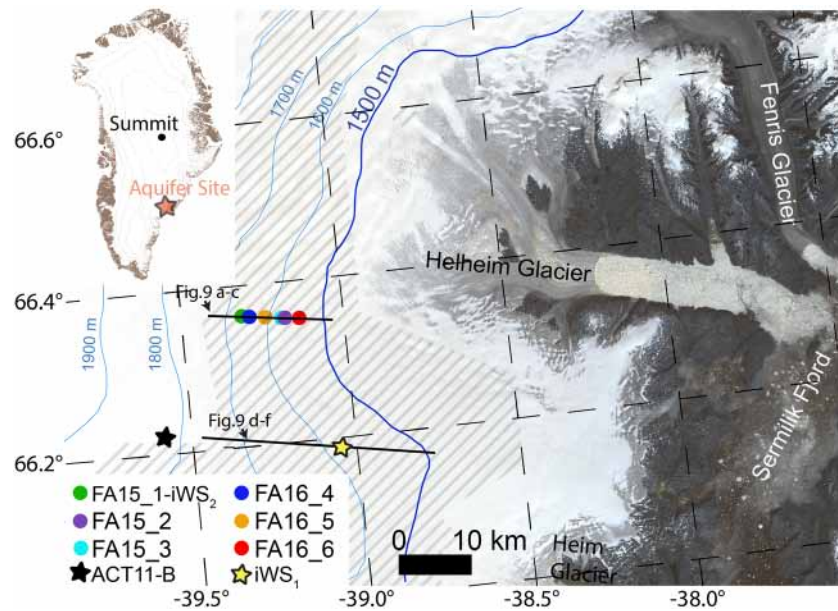
Figure 1. Site map. Landsat-8 composite image (6 August 2017) showing field sites in southeast Greenland visited in April (FA15_1), July, and August 2015 (FA15_2 and FA15_3) and July (FA16_4, FA16_5) and August (FA16_6) 2016, location of ACT11-B core, and location of iWS station prior to relocation at FA15_1. Two black lines represent the airborne radar transects used in Figure 10. Elevation contours from Cryosat-2 DEM (Helm et al., 2014). Gray-stripe area illustrates the presence of firn aquifers inferred from airborne radar data (Miège et al., 2016).

2.2. Field Data Collection and Analysis

Field work for this study included collection of firn and water samples, firn density and stratigraphy data, dye tracing, installation of temperature sensors and pressure transducers in boreholes, and collection of weather data. In April 2011, firn cores from the ACT11-B site (Figure 1) were collected and later transported to the Desert Research Institute lab for chemical analysis following similar methods applied to previous cores from the region (Miège et al., 2013). Longitudinal samples were cut from the cores and analyzed for a range of ~30 elements and chemical species using a well-established continuous ice core analytical system (McConnell et al., 2017, 2002; McConnell, 2020). Annual layer counting based on seasonal variations in the chemical constituents (Sigl et al., 2016) constrained by multiannual to decadal trends in industrial pollution deposition previously documented in well-dated Greenland ice cores (e.g., McConnell & Edwards, 2008) was used to determine the ice core chronologies and develop the depth-age relationship used in the environmental tracer analysis. Annual cycles in the chemistry are largely not preserved due to meltwater infiltration in firn aquifer regions.

Additional field work was conducted in April, July, and August 2015, as well as July and August 2016 at six sites along an ice flow line of Helheim Glacier. To collect depth-specific water samples for environmental tracers and hydraulic measurements (Miller et al., 2019; Miller & Solomon, 2019) to estimate specific yield, a heated piezometer was advanced through the unsaturated firn and aquifer at all six sites (see Miller et al., 2017, for details).

Firn cores were collected to a maximum depth of ~60 m at five of the six sites (minus FA15_3). Each core section (mainly following "natural" breaks in the core but on average less than 20 cm) was measured and weighed for density and its associated stratigraphy (i.e., dry/wet firn, ice lens, bubbly ice, and clear ice) was logged (Koenig & Montgomery, 2019; Miller et al., 2019). These cores were subsampled for tritium measurements. Drilling four of the five boreholes (minus FA15_1) was performed in the summer within mostly temperate (0°C) firn and ice using a custom-made electrothermal drill (Miller et al., 2018). FA15_1 borehole was drilled in the spring of 2015 using a mechanical drill (IDDO SideWinder) for the cold upper firn followed by a 4-inch diameter electrothermal drill (also from IDDO) once temperate firn and ice were reached, similar to drilling operations done by Koenig et al. (2014). Specific conductance (SC) of the water in the aquifer was measured in the open bore holes every 30 cm.

Temperature strings and pressure transducers were installed in the boreholes to record hourly changes in temperature and water levels at FA15_1 and FA15_2 (Miège et al., 2020). A pressure transd/d at FA16_4. The two 50-nodes temperature arrays (Digital ThermArray system from RST ©) were suspended in the boreholes, with one end sitting on the borehole bottom. The temperature arrays sat in water within the saturated zone of the aquifer. The unsaturated zone of the borehole was backfilled with fresh snow. Each temperature sensor came precalibrated (no field calibration required) and had an accuracy of 0.07°C. The sensor vertical distribution with depth varies with a closer (0.5 m) vertical spacing near the surface and wider spacing (5 m) near the bottom.

The water level was monitored with a pressure transducer manufactured by KPSI ©. Each transducer has a precision of 0.1% for a total range of 68.95 kPa. Each transducer is vented at the surface using a small vent tube connected from the transducer to a custom plastic box filled with desiccant on the mast above the surface. Each pressure transducer was deployed about 1 m below the water table to remain in the measurement range for as long as possible in anticipation of water level changes (due to recharge or discharge) on the order of a few meters.

To complement the borehole instrumentation, potentiometers were installed at two sites (FA15_2, FA16_4) to measure overall firn compaction between the snow surface and the water table. At FA15_2, the potentiometer was installed at 0.84 m from the surface on 9 August 2015 and anchored 16.9 m from the surface (2.3 m below the water table). At FA16_4, the potentiometer was installed at 0.70 m from the surface on 29 July 2016 and anchored 13.7 m from the surface (6.4 m above the water table). Additional general details regarding potentiometer setup and firn compaction measurements can be found in MacFerrin (2018). Temperature, pressure transducer, and potentiometer data were stored hourly on a CR-1000 data logger, and 2-hr data were transmitted with a ST-21 Argos transmitter (instruments from Campbell Scientific©).

2.3. Recharge Estimates

2.3.1. Meltwater Generation From Surface Energy Balance and Degree Day Modeling

Surface meltwater generated in 2014, 2015, and 2016 was estimated using both a surface energy balance model, following van den Broeke et al. (2010), and degree-day modeling. An automatic intelligent weather station (iWS) installed in April 2014 collected air temperature, pressure, wind, and incoming and outgoing short and longwave radiation data to calculate energy for melt (Reijmer et al., 2019). The station was relocated on 10 August 2015 from 66.18°N 39.04°W at 1,560 m elevation to a new location ~25 km away along the study profile at 66.36°N 39.31°W at 1,661 m elevation (Figure 1). No correction for this relocation was performed. Gaps in the data set exist because the station was buried by snowfall during the late spring and summer of 2015 and data retrieval in 2016 occurred prior to fall melt cessation. To account for the incomplete melt totals during 2015 and 2016, the melt season was assumed to last 100 days, as it did in 2014. The total calculated melt from the existing data was multiplied by 1.5 for both years to complete the 100 days because the ratio of 100 days to 68 and 65 days of melt for 2015 and 2016 is 1.5. The energy available for melting (M) was calculated as

$$M = SW_{in} + SW_{out} + LW_{in} + LW_{out} + SHF + LHF + G_s \tag{1}$$

where SW_{in} and SW_{out} are incoming and reflected shortwave radiation fluxes, respectively, LW_{in} and LW_{out} are incoming and emitted longwave radiation fluxes, respectively, SHF and LHF are turbulent fluxes of sensible and latent heat, respectively, and G_s is the subsurface conductive heat flux (van den Broeke et al., 2010). Fluxes are defined as positive when energy is added to the snow surface. All radiation fluxes were observed. Latent and sensible heat fluxes were calculated after Andreas (1987). The roughness length for momentum was 0.1 mm, and the roughness lengths for heat and moisture were computed from the roughness length for momentum. Subsurface fluxes were evaluated using snow surface temperature gradient. The absorption of solar radiation in subsurface layers was disabled. The impact of heat diffusion and meltwater infiltration on the temperature of the snowpack were accounted for as well. Additional model details are described in Kuipers Munneke et al. (2018).

The total snowmelt available for recharge was also estimated using a degree day model. The degree day model multiplies time when the air temperature is above a reference temperature (and thus snowmelt can

occur) by a degree day factor (DDF, length time^{-1} temperature^{-1}). Surface melt was calculated using the positive degree day equation (Braithwaite, 1985; Hock, 2003):

$$m = DDF \sum (T - T_0) \Delta t \tag{2}$$

where m is melt (length), T is the air temperature, T_0 is a reference temperature, and Δt is a time interval (1 hr). A range of DDFs calculated for similar latitudes in the ablation zone in SW Greenland were used, and compared for reference temperatures of 273.15 and 268 K (van den Broeke et al., 2010). Melt estimates from the surface energy balance were compared to melt estimates from the degree-day method. The melt estimated from the energy balance model independently constrains DDFs in this area.

The surface melt represents the total amount of water available to recharge the aquifer. However, a fraction of the total melt is retained and refrozen during infiltration through the unsaturated zone and does not reach the aquifer. Recharge to the aquifer (the amount of water that reaches the water table) was estimated using two techniques: the volumetric flow method and the water table fluctuation method.

2.3.2. Darcy/Volumetric Flow Method

Darcy's law is the basis for the volumetric flow method to estimate recharge (Healy, 2010). The volumetric flow was divided by the length and unit width of the aquifer as

$$R_D = \frac{Q}{L\,W} \tag{3}$$

where R_D is the recharge rate (length/time), Q is the volumetric flow of water (length^3/time), L is the length of the aquifer, and W is the unit width through which fluid flows. The flow of water (Q) was estimated using Darcy's law. The water table has an average hydraulic gradient of 0.01 m/m at the study site (Miège et al., 2016). The method assumes that hydraulic conductivity is known across the study area. Hydraulic conductivity is relatively consistent across the study area (geometric mean is 2.7×10^{-4} m/s, geometric standard deviation is 1.6, lower 95% confidence interval is 2.5×10^{-4} m/s, upper 95% confidence interval is 2.9×10^{-4} m/s, Miller et al., 2017). The aquifer thickness at the most downslope site (FA16_6) is 30 to 40 m, and the aquifer length is ~15 km. The average volumetric flow was 8.1×10^{-5} m^3/s, with a lower 95% confidence interval of 7.5×10^{-5} m^3/s and an upper 95% confidence interval of 8.7×10^{-5} m^3/s. Recharge was also estimated using average measured specific discharge from borehole dilution tests reported in Miller et al. (2018). This method also assumes that recharge at every point across the water table contributes to fluid flow through the aquifer and that total recharge to the aquifer is equal to discharge, with no change in storage. This assumption is appropriate at short time scales for this firn aquifer.

2.3.3. Specific Yield and Water Table Fluctuation Method

Recharge was also calculated based on water level changes measured between 22 June 2016 and 12 September 2016 at FA15_1 and FA15_2. Water table fluctuations in boreholes are commonly used to estimate recharge (Risser et al., 2005) as

$$R = S_y \times \Delta h \tag{4}$$

and

$$R_r = S_y \frac{\Delta h}{\Delta t} \tag{5}$$

where R is recharge (length), R_r is recharge rate (length/time), S_y is specific yield, h is water table height (length), and t is time. Aquifer tests, described fully in Miller et al. (2017), were used to determine aquifer specific yield. During an aquifer test, water was pumped from a borehole, and the water level change was recorded in the pumping well and one or two observation wells within 5 m of the pumping well. The specific yield was determined through a curve fitting method described in Miller et al. (2017).

The water table fluctuation method assumes that the specific yield is constant and that the water level rises as recharge water reaches the water table. Water table rises are expected during the melt season if recharge is greater than lateral flow. While the water level can rise for other reasons (changes in atmospheric pressure, earth tides, and entrapped air, which are all expected to have minimal influence on the experiment

timescales), the water level rise in the firn aquifer is assumed to be solely due to recharge. However, lateral flow from upslope also contributes to water level changes and would result in an overestimation of recharge. The opposite is true for downslope lateral flow.

2.3.4. Fluorescein Dye and Recharge Timing

Fluorescein dye was applied to the snow surface to semiquantitively evaluate rates of meltwater travel through the unsaturated zone. After uniformly spraying dye across a 5 m × 5 m area at FA16_4, the borehole was drilled through the center of the area, and the collected firn cores were sampled for dye concentration. Drilling of the borehole is unlikely to affect dye movement; physics governing unsaturated zone flow suggest that capillary pressure retains dye within pore spaces instead of allowing substantial amounts of dye to move along the borehole. Dye concentrations of melted firn core samples were measured at the USGS Utah Water Science Center using a Turner Designs 700 laboratory fluorometer.

2.4. Aquifer Age

2.4.1. Tritium and CFC Ages in Firn and Meltwater

Tritium is a naturally and anthropogenically produced isotope of hydrogen whose concentration in the atmosphere has changed over time because of aboveground nuclear weapons testing. Tritium has a half-life of 12.32 years (Lucas & Unterweger, 2000). Tritium can be used to date waters recharged within the past ~60 years. As part of the water molecule, tritium is a useful tracer of water movement. To date firn and water in the aquifer, the atmospheric tritium signal was matched to the tritium measured in profiles through the aquifer (Cook & Solomon, 1997). This provides a general timeframe of the firn and meltwater (pre- or post-1960s).

Tritium concentration was measured in subsamples of firn cores and water pumped out of the aquifer following the in-growth method at the University of Utah's Dissolved Gas Lab. Tritium concentrations are reported in tritium units (TU) where one TU equals one molecule of $^3H^1HO$ in 10^{18} ^1H_2O molecules. Atmospheric tritium was estimated by decay-correcting measured firn tritium. Sample deposition date was estimated using a depth-age model developed from an ice core taken at ACT11-B similar to Miège et al. (2013). Tritium was also compared to tritium measured at Summit and Dye 3 sites (Fourré et al., 2006; Koide et al., 1982). Tritium concentration varies seasonally in precipitation at Summit, with higher values in the summer and lower values in the winter. Seasonal tritium variations occur due to seasonal atmospheric moisture source variation. Samples were compared to the wintertime precipitation at Summit as the study area does not experience substantial summertime precipitation.

Chlorofluorocarbons (CFCs) are synthetic organic compounds used in a wide range of industrial applications beginning in the 1930s, resulting in widespread release into the atmosphere. CFC-11, CFC-12, and CFC-113 can be used to determine the apparent year water recharges an aquifer. To determine apparent recharge ages, the CFC concentration in a groundwater sample is compared to the known historical (~past 60 years) atmospheric concentration (Elkins et al., 1993; National Oceanic and Atmospheric Administration, n.d.), assuming that the water was in equilibrium with the atmosphere prior to recharge. Concentrations of CFC gases were measured in samples of firn aquifer water on a gas chromatography system at the University of Utah's Dissolved Gas Lab.

2.4.2. Salt Mass Balance Model

The concentration of major ions in central and SE Greenland snow is on the order of 0.18 ± 0.07 mg/L (Oyabu et al., 2016; Yang et al., 1996) with a SC of about 0.3 ± 0.1 μS/cm. In contrast, measured SC of firn-aquifer water ranged from 1 to ~20 μS/cm, or more than 50 times higher than snow SC (Miller et al., 2018). Furthermore, the SC in the firn aquifer is generally at a maximum near the base the aquifer and then drops to below detection below the aquifer base (Miller et al., 2018). In order to understand these observations in the context of the hydrologic measurements, a mass balance of water and dissolved ions in a simple box model was formulated.

The box model is based on the following processes. Impurities such as salts and minerals are present at low levels within the firn due to surface deposition. When meltwater from the surface infiltrates through the firn, it can leach some of these impurities and transport dissolved solids (minerals, salts, or ions) to depth. The related smearing of geochemical records in ice cores by meltwater flow has been observed (Koerner, 1997; van der Wel et al., 2011).
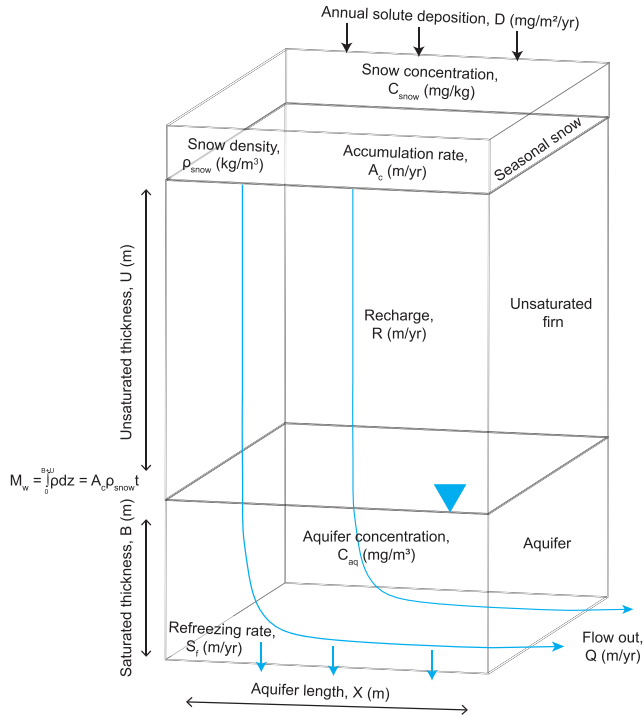
Figure 2. Box model showing salt and water movement through a firn aquifer.

When a firn aquifer forms, the impurities present within the saturated firn dissolve into the liquid water as meltwater infiltration transports additional dissolved solids from above. As freezing at the base of the aquifer occurs due to cold englacial ice temperatures, the dissolved solids are excluded from the ice crystal lattice and instead concentrate in the liquid water of the aquifer. The basal freezing prevents salts from reaching greater depths than normally would occur if the salts remained in place in dry firn following deposition. Meltwater flow transports dissolved solids laterally through the aquifer.

Figure 2 illustrates a box model in which melt water moves vertically through the unsaturated firn into the aquifer, and then either flows out of the box laterally (Q_{out}) or refreezes at the bottom of the aquifer; no water enters from the upstream boundary. The flow of melt water per unit area into the aquifer (recharge) is given by R (m^3/yr/m^2 = m/yr), and the flow that refreezes per unit area is given by S_f (m^3/yr/m^2 = m/yr).

A steady-state water balance is therefore

$$Q_{out} = (R - S_f)WX \qquad (6)$$

where W is the width and X is the length of the aquifer. Major ions in snow have a concentration of C_{snow} (mg$_{salt}$/kg$_{water}$) with a mass flux of D (mg/m^2/yr) and an annual snow accumulation rate of A_c (m/yr). Melt water is assumed to readily leach these salts from the firn, such that the ion concentration in melt water is C_d (mg/m^3) (Bales et al., 1993), and transport salts to the aquifer, that has a porosity of n. A transient salt balance for the aquifer can be written as

$$\frac{d(C_{aq}XBWn)}{dt} = C_d RWX - C_{aq}Q_{out} - C_{ice}S_f WX \qquad (7)$$

Equation 7 states that the time rate of change of solute mass within the aquifer is equal to the solute mass from melt water minus the solute mass that flows out of the aquifer minus the solute mass that is incorporated into ice (set to zero below). This equation assumes that solutes are well-mixed within the aquifer.

Substituting Equation 6 into Equation 7 results in a first-order differential equation with the average solute concentration in the aquifer (C_{aq}) as the dependent variable. A solution to this equation requires an initial condition for C_{aq}. Assuming that all of the solutes in the firn above the bottom of the aquifer are leached into the aquifer water when the aquifer first forms, and assuming that the C_{ice} is zero (i.e., complete ion exclusion in ice that forms from refreezing aquifer water), the solution to the differential equation is

$$C_{aq} = \frac{D}{R - S_f}\left\{1 - \left[1 - \frac{M_w(R - S_f)}{A_c\rho_{snow}Bn}\right]exp\left(\frac{(S_f - R)t}{Bn}\right)\right\} \qquad (8)$$

where C_{aq} is the average concentration in the aquifer, D is the annual solute deposition (mg/m^2/yr), R is the aquifer recharge from melt at the surface (m/yr), S_f is the rate of refreezing on the bottom of the aquifer (m/yr), M_w is the total mass of snow, firn, and aquifer from the aquifer bottom to the surface per unit area (kg/m^2), A_c is the annual accumulation of snow (m/yr), ρ_{snow} is the average snow density (kg/m^3), B is the aquifer thickness (m), n is the aquifer porosity (m^3/m^3), and t is the time since the aquifer formed (yr).

The total mass of snow/firn/aquifer from the aquifer bottom to the surface (M_w) can be computed either by integrating the snow/firn/aquifer density over the distance from the snow surface to the bottom of the aquifer ($B + U$, aquifer thickness plus unsaturated zone thickness), or as the product of the snow accumulation rate (A_c), snow density (ρ_{snow}), and the accumulation time (t_{ac}).

Table 1
Parameter and Uncertainty Values Used in Salt Balance Model

Model parameter abbreviation	Aquifer recharge from melt at the surface R (m/yr)	Aquifer porosity n (m³/m³)	Rate of refreezing on aquifer bottom Sf (m/yr)	Aquifer thickness B (m)	Unsaturated zone thickness U (m)	Annual snow accumulation rate Ac (m/yr)	Concentration of major ions in snow C_{snow} (mg/kg)	Snow density r_{snow} (kg/m³)	Annual solute deposition rate D (mg/m²/yr)
Mean value	0.15	0.07	0.015	12.5	22.5	4	0.32	330	422
Two standard deviations	0.06	0.028	0.006	2.5	4.5	0.8	0.06	66	140

Equation 8 predicts the spatially averaged concentration of solutes in the aquifer as a function of time since the aquifer formed. At time = 0, the aquifer concentration is

$$C_{aq\ t=0} = \frac{DM_w}{A_c \rho_{snow} Bn} \tag{9}$$

which reflects leaching of ions from the snow and unsaturated firn and enriching them in the aquifer water. At time = infinity, the aquifer concentration is

$$C_{aq\ t=\infty} = \frac{D}{R - S_f} \tag{10}$$

which reflects the enrichment of melt water due to ion exclusion on the bottom of the aquifer. The time required to reach about 63% (*e*-folding time) (t_e) of the steady-state concentration is given by

$$t_e = \frac{Bn}{R - S_f} \tag{11}$$

which is the volume of water in the aquifer per unit area divided by the net flow out of the aquifer per unit area. This *e*-folding time is equivalent to the mean residence time of water in the aquifer; small values mean that the initial leaching of ions when the aquifer forms can rapidly be flushed from the system.

Aquifer concentrations were predicted with Equation 8 using parameter values and uncertainties that are shown in Table 1. These parameter values have been constrained by field measurements except for C_{snow} and D that were not measured at study sites. However, Cl, Na, and SO$_4$ concentrations were measured at ACT11b, and the snow pit data of Oyabu et al. (2016) and Yang et al. (1996) were used to estimate the unmeasured ions such as NO$_3$, NH$_4$, Mg, K, and Ca as

$$DS_{ACT11b} = DS_{snowpit}\ x\ \frac{\sum [Cl],\ [SO_4],\ [Na]_{snowpits}}{\sum [Cl],\ [SO_4],\ [Na]_{ACT11b}} \tag{12}$$

where *DS* is dissolved solids, and [*X*] is the concentration of X ion.

2.4.3. Aquifer Extent Mapped Using Airborne Radar Detections

Repeat firn aquifer detections using airborne radar data acquired from NASA OIB were also analyzed to map aquifer extent (2010–2017), following detection methods developed by Miège et al. (2016). This extends the monitoring time from 2010 to 2014 in Miège et al. (2016) through 2017. The water table was identified in the Accumulation Radar data for years 2010–2014 and 2017 and the Multi-Channel Coherent Radar Depth Sounder (MCoRDS) data for 2015–2016 both collected by CReSIS on the NASA OIB airplane (CReSIS, 2017; Lewis et al., 2015; Rodriguez-Morales et al., 2014). The water table is characterized by a high-reflectivity and high-amplitude radar signal due to substantial dielectric contrast between dry firn and water-saturated firn (Miège et al., 2016). The radar two-way travel times from the surface to the water table are converted to depth using an empirical relationship linking the variations of the dielectric permittivity with density variations. An average density profile from several firn-core sites with cores collected from the surface to the water table was used (Miège et al., 2016).

Radar data collected by CReSIS (2017) was used to map aquifer extent prior to OIB data. For Helheim Glacier, airborne radar collection by CReSIS started in the spring of 1993 with a 141.5–158 MHz radar depth sounder. The water table was not visible at this center frequency and with a relatively narrow bandwidth. Instead, the absence of bed returns was used as a proxy to infer the presence of a firn aquifer, as the presence of water in the firn substantially attenuates the radar signal. This relationship was successfully tested using 2010–2014 data when the two radars (Accumulation Radar and MCoRDS) were operating simultaneously on the P-3 airplane, and a clear correlation was observed between the missing bed reflections in the MCoRDS data and the presence of a water-saturated firn layer in the Accumulation Radar (Miège et al., 2016).

3. Results

3.1. Firn Temperature and Melt Generation Patterns

A generalized depth profile of the firn and ice temperatures throughout the year is shown in Figure 3 for the top 55 m of the firn and ice column. The air temperature (Figure 4a) and firn temperature above ~10 m vary seasonally. The firn is coldest in May and then warms throughout June as the surface temperature increases until it becomes temperate (isothermal at 0°C). In 2015, air temperatures rose above 0°C for more than a few hours per day consistently starting 18 June, presumably generating surface meltwater, while in 2016 a similar pattern occurred 16 days earlier (2 June) (Figure 4c). With a time lag of ~27 days and ~20 days for 2015 and 2016, respectively, the water table started rising in response to the melt onset at the surface (Figure 4d). This time lag represents the time required to bring the upper firn to temperate conditions and allow the meltwater to reach the aquifer. Part of the firn-warming process occurs via meltwater refreezing and subsequent release of latent heat in the unsaturated zone. Such short-lived latent heat pulses have been well documented by Humphrey et al. (2012) and can be observed on Figure 4e at 4 m depth in the firn (green line).

Approximately 16 cm of the surface meltwater were refrozen in the unsaturated zone at FA15_1 (from firn temperatures on 9 June 2015) and contributed to warming the seasonal snow and firn to the melting point based on the integrated cold content (e.g., 3.4 in DeWalle & Rango, 2008) of the firn prior to the onset of melt. Data gaps at the onset of melt preclude cold content calculations at the onset of melt (18 June 2015 when air temperatures stayed consistently above 0°C) and at other sites.

The firn remained temperate through August, until air and surface temperatures fell below freezing (Figures 4a and 4f). This slow cooling continues through the fall and winter from the top of the firn column down (Figure 4h) via conduction controlled mainly by air temperature. Snowfall provides insulation, slowing down the cooling process.

The unsaturated firn from 10 m depth to the water table remained temperate year-round in 2016 (Figure 3). The water-saturated firn within the aquifer also remained temperate throughout the year (Figure 3). Below the base of the aquifer (~30 m), the temperature decreases below 0°C (Figure 3). The temperature of the firn controls the location of the impermeable, fully frozen base of the aquifer.

At FA15_2, the lower elevation site (1,543 m), the ice temperature below the aquifer at 55 m from the snow surface is warmer by 1.2°C on average compared to FA15_1, the upper elevation site (1,664 m). The freezing depth below the aquifer is found about 5 m deeper at FA15_2 (~40 m from the surface) compared to ~35 m for FA15_1 (Figure 3). The exact freezing depth could not be determined due to the 5-m spacing of the temperature sensors at these depths (Figure 3).

3.2. Melt, Infiltration, and Recharge Estimates

3.2.1. Meltwater Generation From Surface Energy Balance and Degree Day Models

The surface energy balance (Equation 1) model suggests that between 24 and 50 cm of meltwater per year (from 2014 to 2016) were generated at the snow surface (Figure 5). The meltwater estimated from the degree day modeling, which ranges between 31 and 156 cm, is summarized in Table 2.

The melt rates from the energy balance model estimates constrain appropriate DDFs (those that result in similar melt) for this site to lower values of 1 to 1.5 mm day^{-1} K^{-1} for a reference temperature of 268 K or 8 to 10 mm day^{-1} K^{-1} for a reference temperature of 273.15 K. These DDFs result in between 31 to 78 cm of melt.
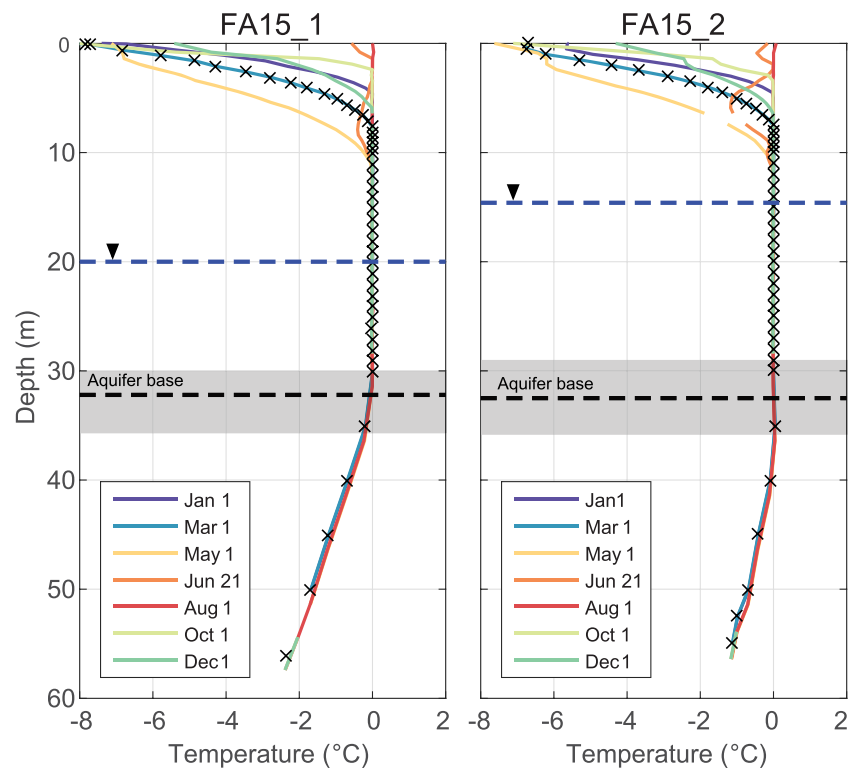
Figure 3. Firn temperature profile evolution from January 2016 to December 2016 at (left) FAI5_1 and (right) FA15_2. Depths refer to sensor depths in 2016 and account for subsequent snowfall and melt following installation in 2015. Black triangle indicates water table depth, and black dashed line represents aquifer base depth in August 2015. Gray shading indicates uncertainty in aquifer base depths. Black x indicates sensor locations. Vertical resolution varies with depth. The depth to the water table was determined using the steel tape method (Garber & Koopman, 1968) and the depth to the aquifer base was determined with active source seismology (Montgomery et al., 2017).

The surface melt estimates represent the total available water at the snow surface that could infiltrate through the unsaturated zone and recharge the aquifer. As some melt is refrozen in the unsaturated zone as described in section 3.1, the actual amount of water that recharges the aquifer is less than the total melt generated at the snow surface. This is shown in Figure 5, which compares the total amount of meltwater generated at the surface with the estimates of water that recharges the aquifer. The recharge cannot be greater than the total melt generated.

3.2.2. Infiltration Rates
Some dye sprayed on the snow surface reached the aquifer in less than 2 days (breakthrough time). It took 49 hr to drill to the water table at 20 m, and the firn sample collected at the water table contained measurable amounts of dye (Figure 6a). This represents a minimum travel time for the initial breakthrough of dye through the unsaturated zone. Some dye could have reached the water table in less time, but drilling was too slow to determine this. Therefore, the infiltration rate of surface meltwater to the top of the aquifer is generally <0.4 m/hr (calculated as 20 m/49 hr).

3.2.3. Recharge From Volumetric Flow Method
The recharge estimated using the volumetric flow method ranges between 16 and 24 cm/yr, depending on the hydraulic conductivity and aquifer thickness at the downhill edge of the aquifer (Table 3) for a profile 15 km long. This recharge rate is slightly less than the 27 to 36 cm/yr predicted by the average specific discharge from borehole dilution tests or the 35 to 47 cm/yr predicted by the specific discharge at FA16_6 for a thickness of 30 and 40 m, respectively (Miller et al., 2018; Montgomery et al., 2017). As expected, these recharge estimates are lower than the available melt estimated using the Degree Day Method.

3.2.4. Recharge From Specific Yield and Water Table Fluctuation Methods
The portion of the total meltwater that recharges the aquifer can contribute to water level rise. Figure 4 shows the observed interannual variability of water-level changes (FA15_1 and FA15_2) and the air
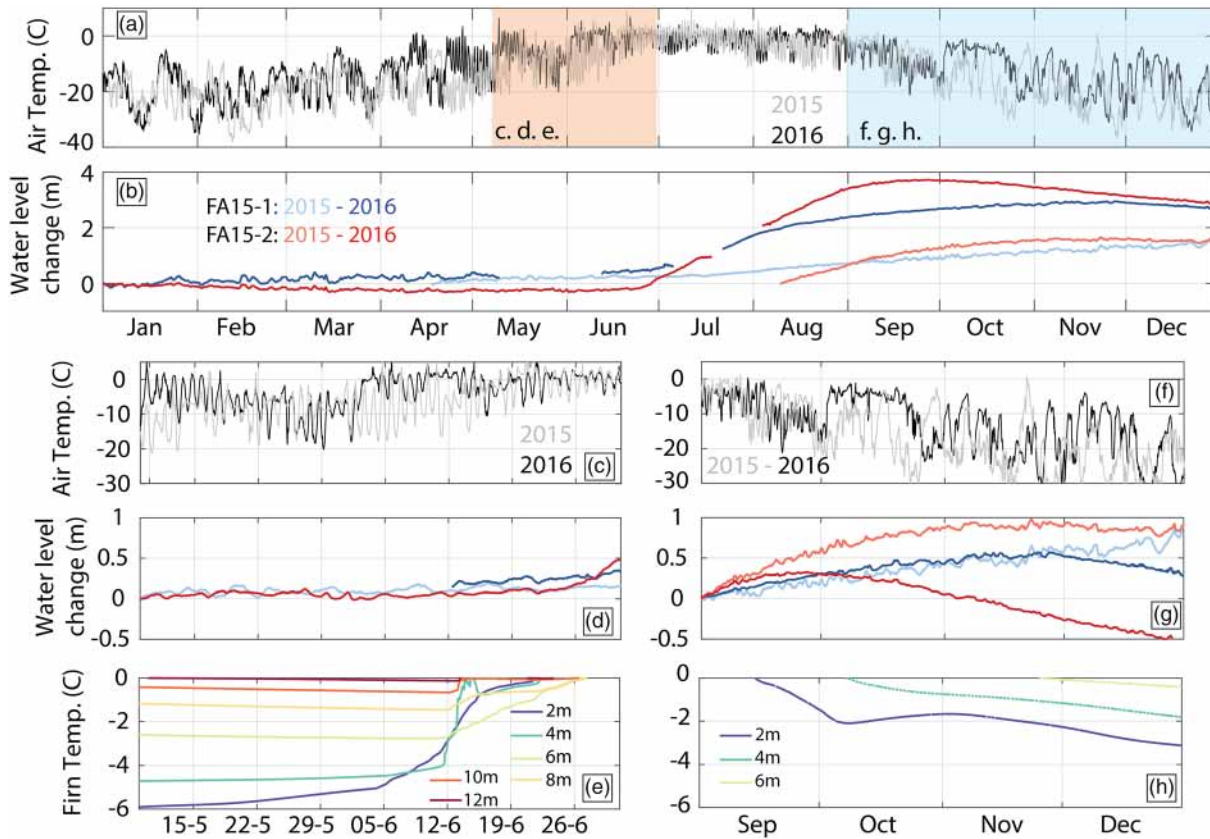
Figure 4. Air temperature, water level, and firn temperature evolution for the duration of the monitoring (2015–2016). Panel (a) represents the air temperature at FA15_1 for one year with 2015 in gray and 2016 in black. Panel (b) represents the relative water-level changes also for 2015 and 2016 at the two monitoring sites: FA15_1 in light blue for 2015 and dark blue for 2016 and FA15_2 in light red for 2015 and dark red for 2016. Note that the zero is set during station setup (17 April 2015 for FA15_1 and 9 August 2015 for FA15_2) and reset to zero on 1 January 2016 for both sites. Panels (c), (d), and (e) correspond to the melt onset period highlighted in (a). Water level changes in (d) are relative to the water level on 9 May. Panels (f), (g), and (h) correspond to the cooling period highlighted in (a). Water level changes in (g) are relative to 1 September. Firn temperatures shown in (e) and (h) represent 2016 only, and the associated measurement depths do not include the seasonal snow cover. For panel (e), dates are indicated as day-month (DD-M).

temperature (FA15_1), with temporal close ups highlighting the melt onset (late May to early June) and firn cooling in the Fall/Winter. During the melt season, the water table rises, presumably as recharge is greater than lateral flow (Figures 4b and 4d). During the rest of the year, lateral flow removes the seasonal input and the water table can drop (Figure 4b and 4g).

Figure 4g illustrates the variability of the water-table evolution between the two sites (FA15_1 and FA15_2) and between 2015 and 2016. The water-table yearly maximum was reached earlier in 2016 than 2015 at both sites. At FA15_2, the maxima occurred on 23 November 2015, and 28 September 2016. At FA15_1, the maximum occurred on 21 November 2015, and no clear maximum occurred in 2016. Also, the relative water-level rise was greater in 2016 compared to 2015, which is in agreement with the increased amount of meltwater produced at the surface that year. These measurements do not account for surface compaction, which was measured to be 32 cm for the upper 16 m of the firn, averaged from August 2015 to August 2016 but close to 0 from 1 June until 1 September 2016, and therefore would not substantially impact the recharge estimates.

In 2016, the water level began to rise on 22 June at FA15_2 (Figure 4) once all unsaturated zone temperature sensors started reading melting-point temperatures. Meltwater recharged the aquifer until mid-September, when surface temperatures cooled below 0°C and meltwater generation ceased for the season. The water level continued to rise after the cessation of surface melt due to drainage of the overlying unsaturated firn for a few days (Figure 4).
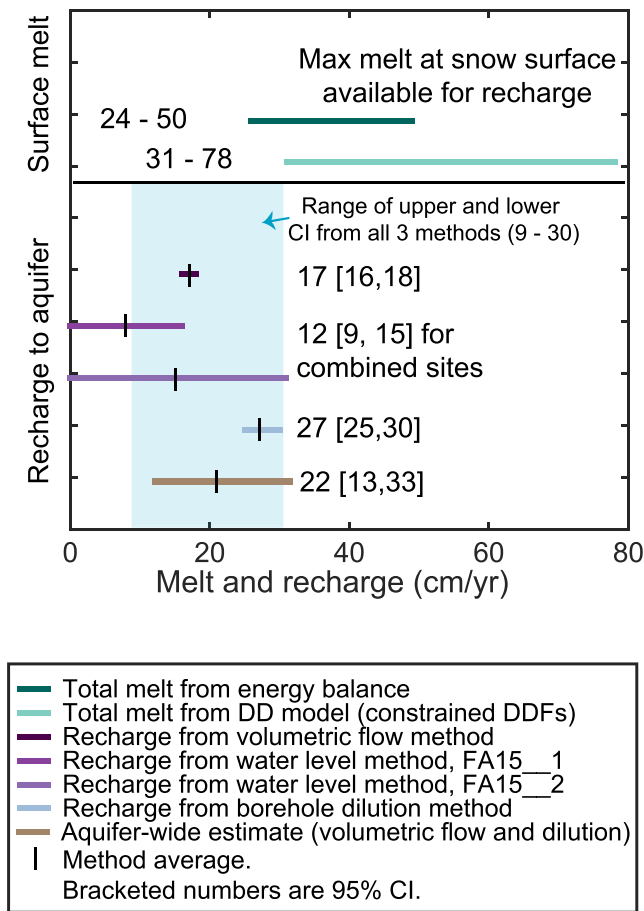
Figure 5. Comparison of surface melt calculated from an energy balance model, total melt generated from degree day modeling (using DDFs constrained by melt from the energy balance), and average and 95% confidence interval estimates (in brackets []) of recharge to the aquifer using the volumetric flow, water level, and borehole dilution methods, assuming a 30 m thick aquifer and a specific yield of 0.04. The range of surface melt estimates represent the range of parameters used in calculations. The total available meltwater from the degree day model is the maximum possible water that could recharge the aquifer. Surface melt is generally greater than the recharge estimates due to retention of meltwater in the unsaturated zone through freezing. Water that freezes in the unsaturated zone does not contribute to recharge of the aquifer.

The water table continued to rise throughout the fall. It is unlikely that this continued rise results from drainage of the unsaturated zone due to the short time (days) water takes to move through the unsaturated zone (Figure 6). Therefore, lateral flow of water from upslope, following local topography, likely contributes to the long (weeks to months) continued water table rise.

The water level rose nearly 4 m at FA15_2, and about 2 m at FA15_1 between 22 June and 12 September 2016 (Figure 4b), indicating that more recharge occurred at the lower elevation site, assuming uniform specific yield. This is a reasonable assumption because the hydraulic conductivity is relatively homogeneous laterally. Increased melt at lower elevations (and warmer temperatures) may contribute to this increased recharge.

The specific yield is shown in Table 4. The firn aquifer has a relatively high hydraulic conductivity, similar to an unconsolidated sandy aquifer (Miller et al., 2017). Consequently, the water table was only lowered several centimeters to a meter during aquifer tests. The size of the pump was limited by the size of the borehole which in turn was limited by the size of the portable thermal drill and the logistics of transporting equipment onto the ice. This weak perturbation of the system made constraining the specific yield difficult. The error on the average specific yield results in high errors on the mean recharge using the water level change method. Still, specific yield appears generally low, with an average of 0.04, excluding the 0.22 value as an outlier, and 0.06 including the 0.22 value. For an intermediate specific yield of 0.05, recharge at the two sites ranges between 11 and 19 cm/yr (Table 5).

The total recharge for specific yields between 0.01 and 0.20 ranges from ~2 to 77 cm/yr (Table 5). These estimates are consistent with or higher than the recharge estimates using the volumetric flow method. They are consistent with or lower than the meltwater available for infiltration estimated using the Degree Day Method. The melt generation and recharge results are summarized and compared in Figure 5.

3.3. Aquifer Time Scales
3.3.1. Tritium

Tritium measurements of liquid water show that the water in the aquifer is modern (i.e., it recharged after ~1960). The measured ^{3}H concentrations in firn and water samples are shown in Figure 7. In the spring of 2015 at FA15_1, prior to the onset of melt, the tritium in the water was similar to tritium in the surrounding firn (Figure 7a), suggesting that the liquid water and firn were in isotopic equilibrium. During the summer, recharge from surface

Table 2
Melt Available to Recharge the Aquifer

Degree day factor (Tref = 273.15 K) (mm/d K)	Melt (cm)			Degree day factor (Tref = 268 K) (mm/d K)	Melt (cm)		
	2014	2015	2016		2014	2015	2016
8	62	31	39	1	45	31	32
10	78	39	48	1.5	68	46	47
20	156	79	97	2	90	61	63

Note. Two reference temperatures were used, following van den Broeke et al. (2010).
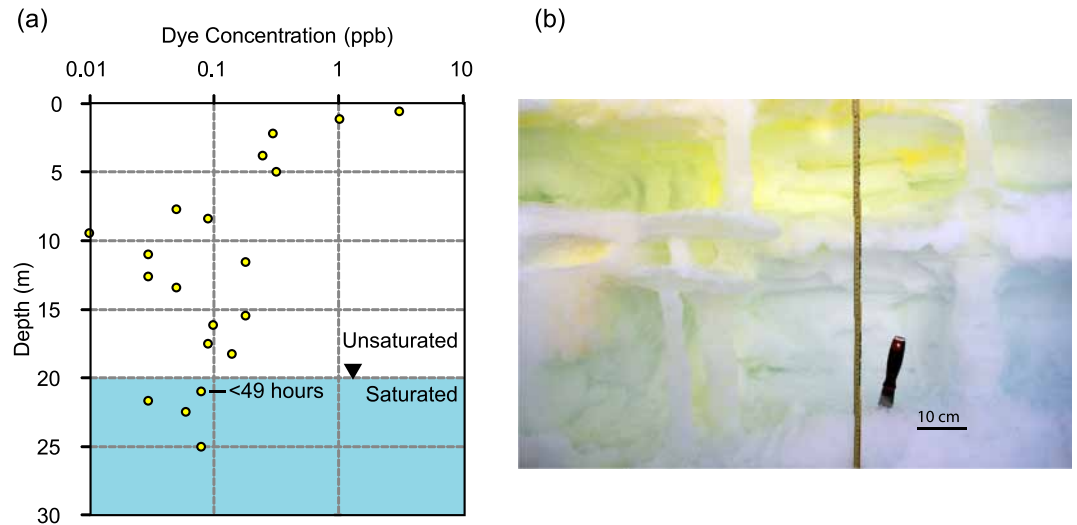
Figure 6. Dye infiltration through firn. Plot showing dye concentration at depth within the unsaturated and saturated firn and minimum time dye took to reach the water table (a) and photo of piping observed in the wall of a snow pit (b). Dye was present when the drill reached the water table after 49 hr. The yellow dye in the photo (b) was sprayed on the snow surface. Measuring tape is in cm. Ice columns in the photo range between ~5 and 30 cm in length and average ~5 cm in diameter.

meltwater, which has a higher tritium concentration, mixes with liquid water in the aquifer and causes the tritium in the liquid water to increase above the firn (Figure 7b). Tritium in firn at depth has experienced longer periods of radioactive decay, resulting in lower tritium concentrations. This indicates that the aquifer is indeed recharged by surface meltwater infiltrating through the unsaturated firn above the aquifer.

At the time of deposition, the decay-corrected tritium in firn at the study sites is similar to the winter time tritium at Summit, a high-elevation long-term research site in central Greenland (Figures 1 and 7c) (Fourré et al., 2006). After ~1990, the tritium signal becomes constant at ~9 TU (Figure 7c). As a result, dating shallow firn cores becomes simple as the concentration in firn only depends on the decay over time and requires only a few samples. This relatively constant input, combined with tritium decay, results in the observed tritium decrease with depth. The samples integrate ~30 cm of firn and therefore contribute to smoothing of any seasonal signal. Additionally, meltwater percolation through the firn contributes to smoothing of the seasonal signals. Within the aquifer, all seasonal signals are smoothed out. Below the aquifer in the solid ice, the tritium concentration begins to increase as expected, approaching the bomb peak. Peak atmospheric tritium concentrations occurred in 1963, but the thermal drill was equipped with a 60-m cable and was therefore not capable of reaching ice below a depth corresponding to the early 1970s.

3.3.2. Chlorofluorocarbon Dating

CFC-11 concentrations and apparent recharge years for each site are shown in Figure 8. CFC-12 and CFC-113 were also measured and show similar patterns. The concentration and apparent age generally decrease with depth. However, the estimated water ages show an unusual pattern with respect to the firn age; the water appears older than the firn, suggesting that the water recharged before the firn in which it now resides was deposited. This unusual, and obviously nonsensical, age relationship implies that the traditional CFC dating model does not apply to firn aquifers, but still provides insights into water movement in the unsaturated firn (see section 4).

3.3.3. Aquifer Formation Timing and Expansion

In addition to explaining the elevated specific conductance of aquifer water relative to melted snow, the salt mass balance model also constrains aquifer formation timing. Figure 9 shows the aquifer concentrations predicted with Equation 8 using parameter values and uncertainties shown in Table 1.

Table 3
Recharge Estimates Using the Volumetric Flow Method

Aquifer thickness (m)	Recharge rate (cm/yr) for hydraulic conductivity (m/s) of		
	2.5×10^{-4}	2.7×10^{-4}	2.9×10^{-4}
	Lower bound of 95% confidence interval	Mean	Upper bound of 95% confidence interval
30	16	17	18
40	21	23	24

Table 4
Specific Yield Estimates at FA16_5 and FA16_6

Site		Well	Specific yield
FA16_4	Test 1	Observation 1	0.01
	Test 2	Observation 1	0.01
FA16_6	Test 1	Pumping	0.03
		Observation 1	0.22
		Observation 2	0.06
	Test 2	Pumping	0.06
		Observation 1	0.05
		Observation 2	0.04

Because the model (Equation 8) predicts the average concentration over the spatial (both vertical and horizontal) extent of the aquifer, it is not expected to reproduce the concentration at specific points. The average SC measured in at sites FA16_4, FA16_5, and FA16_6 is about 6 μS/cm, and this is consistent with an average aquifer formation time of about 16 years (−6, + infinity), based on Equation 8. This corresponds to a formation year of 2000, or as recent as 2006, or as old as the ice sheet. The positive uncertainty in this time is large due to uncertainty in model parameters and the flattening of the concentration versus time curve. However, the upper range of uncertainty on age is constrained by the post-1960s tritium age to +37 years, assuming a 1963 bomb peak.

The lack of bed returns in CReSIS radar data, a proxy for firn-aquifer presence (shown in Miège et al., 2016, Figure 4), indicates that the aquifer existed in 1992. This provides an independent confirmation that an average formation time of 16 years seems to be at least within the correct order of magnitude. Moreover, the parameter values in Table 1 give an average initial SC of about 16 μS/cm, a final (steady state) value of 5 μS/cm, and an *e*-folding time of 6.5 ± 4 years. The uncertainty is based on propagation of uncertainty values for parameters used to calculate the e-folding time in Table 1. These modeled values are within the range of measured values for SC, and the *e*-folding time is similar to estimates of the mean residence time of water in the aquifer estimated using porosity and recharge rates (Miller et al., 2018).

Of course, the salt-balance box model has several limitations including assumptions of steady flow, average concentrations, and instantaneous leaching of salts, in addition to uncertainty in the solute deposition at our study site. Nevertheless, it does explain the approximately fiftyfold enrichment of aquifer concentrations over snow melt, and the general time scale over which solute concentrations are expected to change. Furthermore, the model places a constraint on the fraction of recharge that refreezes at the aquifer bottom. For example, if 90% of the recharge were refreezing, the model predicts a steady state SC of 47 μS/cm and an *e*-folding time of 58 years, both of which are significantly greater than our observations. The model also provides additional evidence that the estimate of recharge (*R*) is reasonable as it is consistent with both hydraulic and chemical observations which are independent of each other.

Repeat perennial firn aquifer detections using airborne radar data acquired from NASA OIB provide an independent set of observations of recent (2010–2017) aquifer expansion upslope (Figure 10). Two water-table time series between 2010 and 2017 in the proximity of the field site are presented (Figure 10). The first water-table time series (Figures 10a–10c) was collected over a transect where most field measurements described in this manuscript took place (aquifer-site transect). From April of 2010 to 2017, the firn aquifer has expanded 7 km inland toward higher elevations. The second time series (Figures 10d–10f), collected on a parallel transect about 30 km south of the first transect, shows a similar upslope expansion of

Table 5
Recharge Rates from Water Level Rise Method

	Recharge rate at site			
	FA15_1		FA15_2	
Specific yield	Recharge rate (cm/day)	Total recharge (cm/yr)	Recharge rate (cm/day)	Total recharge (cm/yr)
0.01	0.03	2	0.05	4
0.04 (aquifer average)	0.10	8	0.19	16
0.05	0.13	11	0.24	20
0.1	0.25	21	0.47	39
0.2	0.51	42	0.95	78
Total water level rise (m)	2.1		3.9	

Note. This table shows water level rise over the 82-day period of meltwater recharge to the aquifer, total annual recharge, and recharge rate for a range of specific yields at FA15_1 and FA15_2. The water level began to rise on 22 June 2016. The last day of substantial melt was 12 September 2016. After this day, air temperatures were too cold for melt to occur.
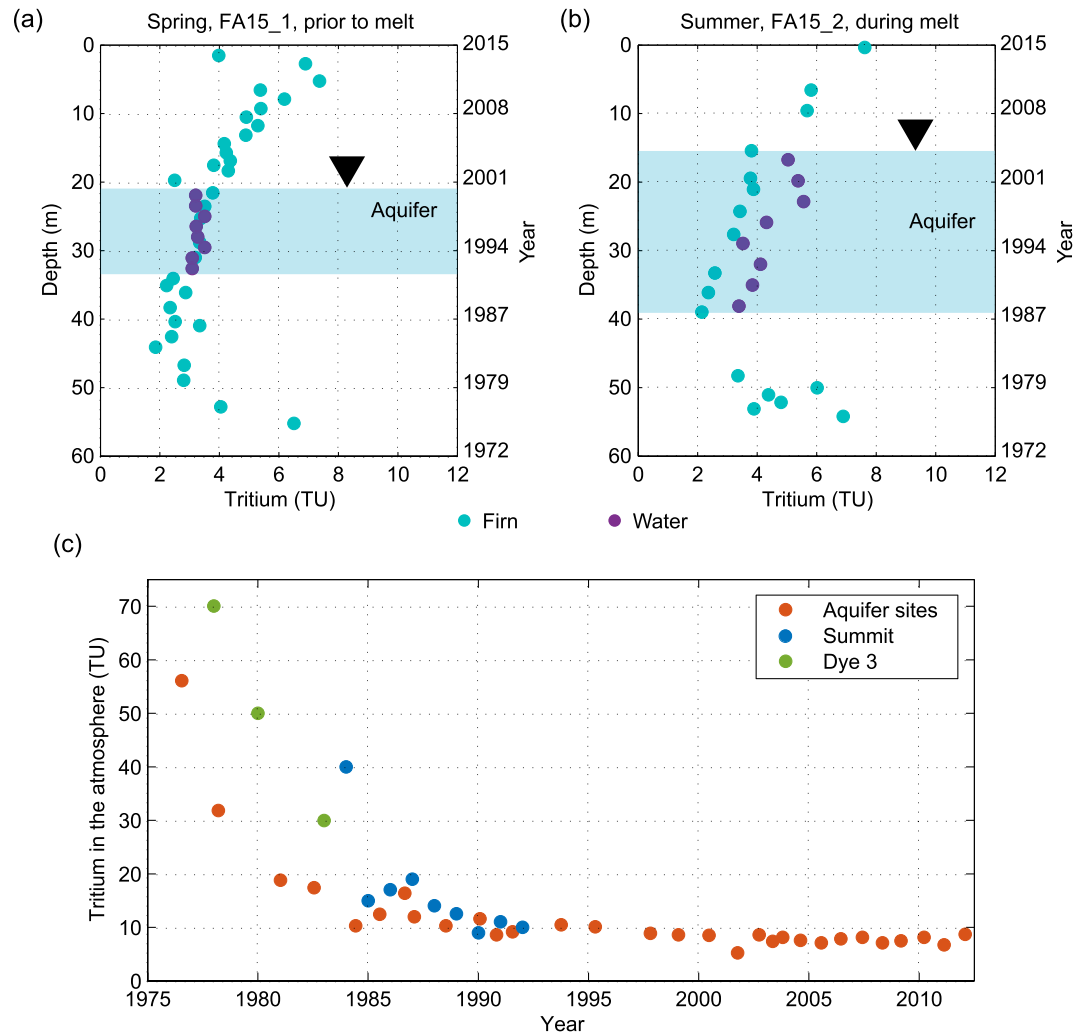
Figure 7. Tritium measured in firn and water at depth in the spring (a) and summer (b), and tritium at the time of deposition (decay-corrected) calculated from firn samples at the field sites compared to tritium in the atmosphere at Summit (GRIP site, 72°N, 37°W) and Dye 3 (65°N, 43°W) Greenland from Fourré et al. (2006) and Koide et al. (1982) (c) Core depth model was developed from the ACT-11B core. Over the winter, tritium in water equilibrates with tritium in firn. The tritium in liquid water increases in the summer due to recharge of surface meltwater.

5 km since April of 2011. This aquifer expansion is presumably driven by increasing surface melt conditions at higher elevations.

The radar data highlights that the water table is controlled by local topography similar to Tóth (1963). In addition, from 2010 to 2017, the upper-elevation part of the aquifer rose (depth to water table has decreased) while the lower-elevation part, delineated by dashed vertical line in Figure 10, lowered (depth to water table has increased). A change in surface slope corresponds to these diverging behaviors. For the aquifer-site transect (Figure 10a–10c), independent magnetic resonance soundings show that the water volume stored at the transition between upper and lower parts of the aquifer is the smallest (~200 kg/m^2) (Legchenko et al., 2018a). These observations confirm the importance of surface slope in controlling the firn aquifer water table lateral evolution and dynamics, just as it has been observed in groundwater aquifers.

4. Discussion

The results from the wide variety of measurements lead to some specific inferences about relative timing of formation and recharge to the firn aquifer. Combined with prior work on the aquifer, they also provide the basis for a broad generalization of a conceptual model.
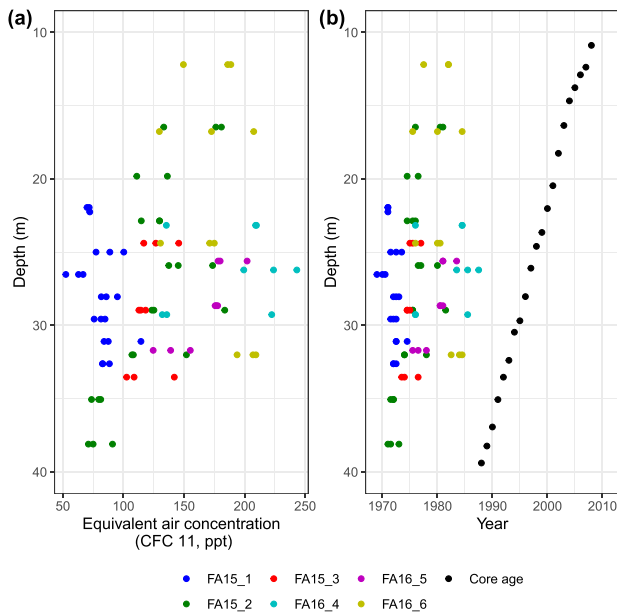
Figure 8. CFC-11 concentrations and model ages. Concentration of CFC-11 (a) and apparent recharge year compared to firn core age model from ACT-11B (b) for all sites. The CFC concentrations are used to calculate apparent recharge years. The calculated apparent recharge year is older than the core age, suggesting that the traditional CFC dating model does not apply here, because melt water does not equilibrate with atmospheric CFCs.

Figure 9. Aquifer solute concentration (as specific conductance) predicted using Equation 8 with parameter values and uncertainties shown in Table 1.

4.1. Relative Timing of Aquifer Formation

The temperature profiles below the aquifer at the higher (FA15_1) and lower elevation (FA15_2) sites provide insight into the relative timing of the aquifer formation. The 1.2°C warmer temperature at 55 m depth for the lower elevation site suggests that the firn aquifer formed earlier at the lower site. This allowed temperate conditions and heat from the aquifer to propagate downward during the densification process over a longer period of time, resulting in warmer temperatures (Figure 3). This hypothesis is also supported by the additional amount of clear ice observed below the firn aquifer at the lower site compared to the higher site, highlighting that the aquifer has persisted for a longer time at the lower site (Miller et al., 2018).

4.2. Meltwater Movement Through the Unsaturated Zone

The dye test illustrates the melt water infiltration pattern of recharge and allows a quantitative comparison of the rate with other percolation settings. Dispersion and the physics of flow through unsaturated porous media cause the dye concentration to decrease with depth (Figure 6a). The increased variation in the concentration at depth suggests that flow occurs along preferential flow paths. This is corroborated by piping identified in snow pits (Figure 6b). The upper bound of the infiltration rate (< 0.4 m/hr) is at the high end of the observed range of vertical percolation velocities between 0.1 and 0.4 m/hr in mountain-glacier firn (Ambach et al., 1981; Oerter & Moser, 1982; Vallon et al., 1976; Schneider, 1999).

CFC results also provide evidence for rapid infiltration rates. Under the traditional CFC dating model, water equilibrates with atmospheric gases above the land surface or unsaturated zone atmosphere. The water then maintains that equilibrium concentration after it recharges a terrestrial aquifer. However, in the case of a firn aquifer, CFCs gases are essentially excluded from ice. Because of size exclusions, the solubility of gases (with the exception of small gases such as helium) is much lower in ice than in liquid water (Bari & Hallett, 1974; Lovely et al., 2015). When the ice melts, it recharges the aquifer before atmospheric equilibration can occur, causing recharge to the aquifer to have very low CFC concentrations (and therefore older apparent recharge years). Once meltwater is in the saturated zone, the only gas that can dissolve into the water is gas present in pore space. While this may increase the CFC concentration in the water, the volume is too small to raise the concentration in the water enough to appear even as old as the firn. Therefore, although CFC apparent recharge years cannot be determined, the unusually low gas concentrations suggest that recharge occurs quickly (faster than CFC equilibration time on the order of hours to days, depending on the surface area to volume ratio).

4.3. Recharge Rates

Recharge to the aquifer is generally estimated to be between 9 and 30 cm/yr across methods, as shown in Figure 5. This estimate is based on the lowest and highest 95% confidence interval of the three independent methods used to estimate recharge. The estimates from the water level change are site specific, while the volumetric flow and dilution methods are averaged over the length of the aquifer and
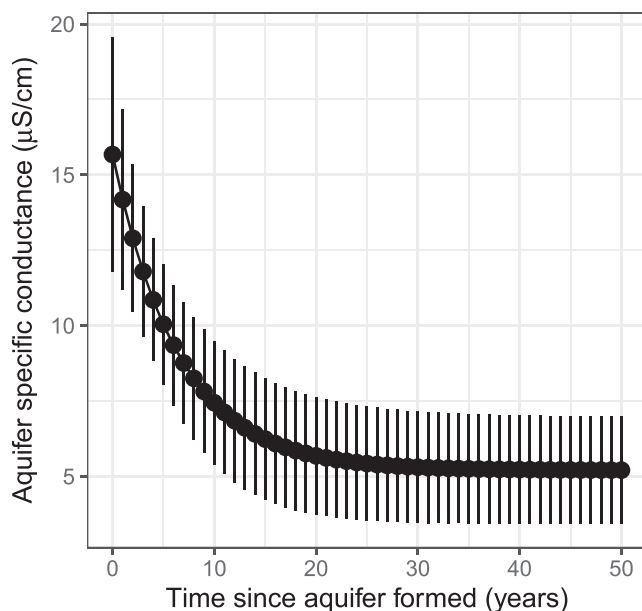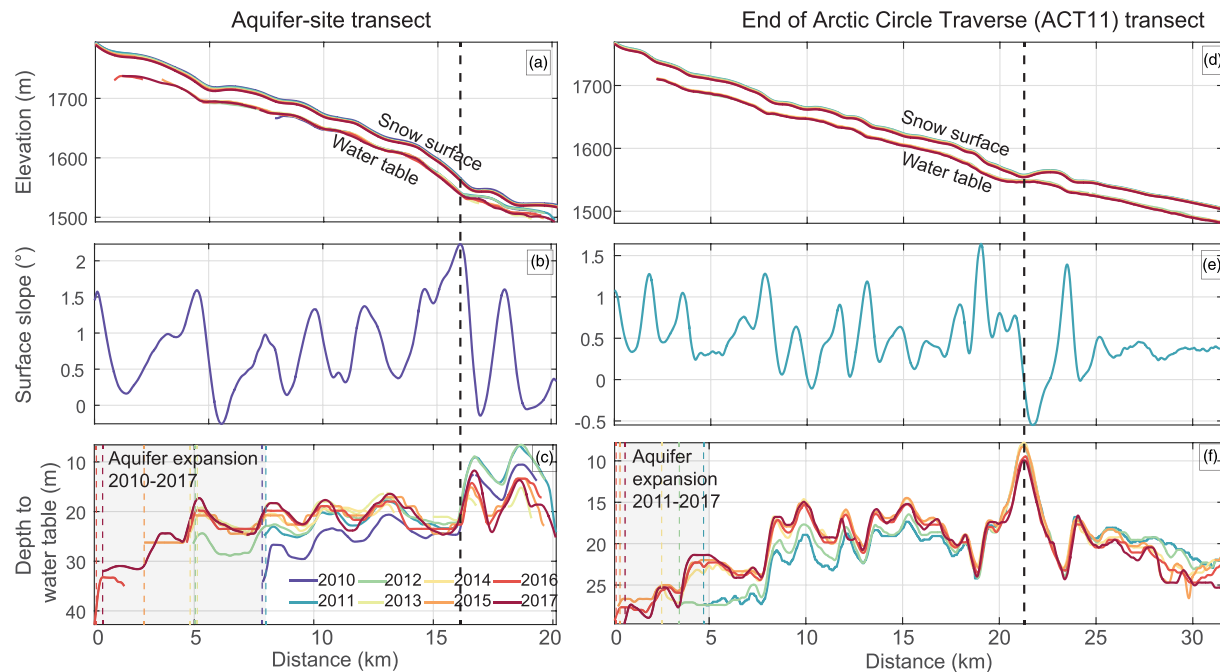
Figure 10. Firn aquifer expansion detected from repeat airborne radar/lidar data (CReSIS, 2017; Studinger, 2020) collected by NASA OIB (2010–2017) at two locations (Figure 1) by Helheim Glacier. The three left insets (a–c) correspond to radar/lidar time series collected at the northern aquifer site transect, whereas the three right insets (d–f) represent radar/lidar time series collected on the transect at the end of the Arctic Circle Traverse from 2011 (ACT11), parallel and ~30 km south of the first transect. Dashed line indicates transition from a rising water table (left of line) to a falling water table (right of line). The surface slope is initially calculated over 0.5 m (radar trace spacing) in average but smoothed using a spline curve.

therefore provide a more general estimate. Further, the agreement between the specific discharge estimated from Darcy's law and the borehole dilution tests (Miller et al., 2018) supports the recharge estimate calculated using the volumetric flow method with the mean hydraulic conductivity and the recharge estimates from the borehole dilution method. The aquifer-wide average recharge from the volumetric flow and borehole dilution methods is 22 cm/yr, with a lower 95% confidence limit of 13 cm/yr and an upper 95% confidence limit of 33 cm/yr (Figure 5). The average of all methods is 18 cm/yr, with an upper 95% confidence interval of 28 cm/yr and a lower 95% confidence interval of 8 cm/yr.

Recharge rates vary spatially. The recharge estimate at FA15_2 is nearly double that at FA15_1, using the water level rise method. The specific discharge at the lowermost elevation site, FA16_6, results in a recharge rate of 35 cm/yr. Recharge decreases with elevation. This is consistent with spatially varying snow surface temperatures and melt rates along an elevation gradient.

The difference between the total melt and the recharge estimates allows for an independent estimate of the amount of refreezing in the firn, assuming that all meltwater that did not contribute to recharge refroze (and reduced pore space) in the seasonal snow from the previous winter or the unsaturated firn. The difference between melt and recharge ranges between 0 and 45 cm. This range is the difference between the maximum aquifer-wide recharge estimate and the minimum melt available for recharge based on the energy balance and the difference between the maximum melt available for recharge based on energy balance and the minimum aquifer-wide recharge estimate. This range is roughly consistent with the integrated cold content estimation requiring ~16 cm of meltwater refreezing to warm the unsaturated seasonal snow and firn to its melting point. The cold content is a conservative estimate that ignores shallow firn warming through conduction, and only represents one site. Each measurement included in these estimates has uncertainties and potential temporal and spatial variability, and so these initial recharge estimates require further work, especially refining measurements of specific yield, which contribute substantially to the uncertainty.

4.4. Conceptual Model

The perennial firn aquifer conceptual model (Figure 11) provides a unifying description of interpreted field data and cryohydrologic/geochemical processes that allow the firn aquifer to persist. For the aquifer to form
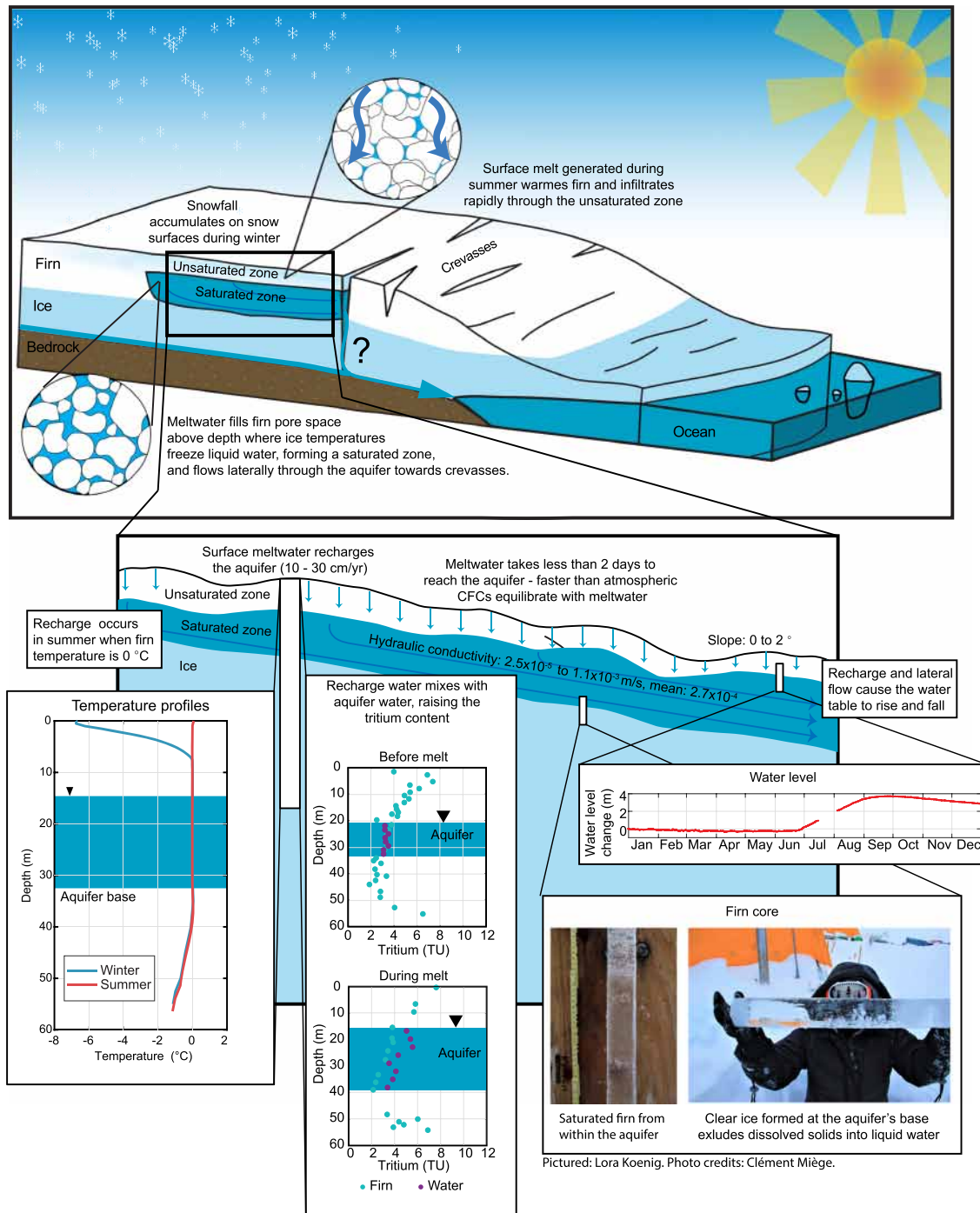
Figure 11. Conceptual model of the firn aquifer. Snow accumulates during the winter on the surface of the ice sheet. In the summer, the warm air temperatures and intense solar radiation cause some of the surface snow to melt. The meltwater warms the firn pack (which is cold—several degrees below 0—due to winter chilling) as it infiltrates and refreezes until unsaturated zone temperatures rise toward 0°C. For firn temperatures just below and near zero, the meltwater can pass through the unsaturated zone and recharge the water table of the firn aquifer. The aquifer is perched upon colder impermeable glacial ice, and this firn aquifer base occurs where all water is fully frozen. The depth of the base is temperature dependent (i.e., it is a function of the depth at which firn temperature is below 0°C), and the temperature distribution depends on the energy balance between conduction in the colder ice sheet and energy conduction and possible advection of energy within the aquifer. Liquid water in the firn aquifer flows relatively quickly through the aquifer to discharge points, likely in crevasses toward the distal end of the ice sheet.

initially, a substantial volume of meltwater must infiltrate to depth. This volume must contain enough thermal energy to warm the firn at depth to 0°C through refreezing, with enough water remaining in liquid form for the aquifer to persist until the next melt season. Recharge was likely lower in the past, and has presumably increased as melt has increased over time (Fettweis et al., 2011). Therefore, recharge rates high enough to currently maintain an aquifer were probably adequate to initiate formation, based on the current presence of an aquifer. This low required amount of recharge suggests that even slight increases could allow for widespread aquifer expansion at locations where adequate pore space exists. The firn-warming process may have initially taken several melt seasons, depending on the amount of melt generated each year. Once this initial energy barrier was overcome, and the aquifer temperature reached 0°C, the aquifer could persist if energy derived from meltwater recharge balanced or exceeded the thermal energy loss from the aquifer.

During the fall, winter, and spring, surface temperatures and incident radiation are too low to generate meltwater. Once summer warming and long days allow for meltwater generation, initial meltwater (~16 cm) contributes to warming of the unsaturated firn overlying the firn aquifer. During this time, refreezing of meltwater contributes to warming of the firn column through latent heat exchange and internal energy accumulation (Schneider & Jansson, 2004). When the overlying firn finally becomes approximately isothermal at 0°C after ~1 month, surface meltwater can rapidly recharge the aquifer. Annual recharge is critical to aquifer persistence. Without it, the aquifer would presumably refreeze due to the surrounding sub-freezing firn temperatures.

Recharge amount and timing estimates from a variety of methods all generally agree that recharge amounts range from 9 to 30 cm/yr. The portion of the surface melt that does not refreeze in the firn infiltrates through the ~10 to 20 m of unsaturated firn along preferential flow paths to recharge the aquifer in at least 2 days. This recharge occurs too quickly for CFCs in the atmosphere to equilibrate with meltwater. However, tritium, as part of the water molecule, is conserved in liquid water, although some vertical smearing in firn occurs. Recharge continues through the summer season as surface melt occurs. Recharge and horizontal flow in the saturated zone contribute to changes in water table elevation. The firn aquifer responds dynamically to surface forcing. This supports findings of Chu et al. (2018), who identified annual changes in aquifer thickness that corresponded to changes in surface mass balance.

Drainage from the unsaturated zone and subsequent changes in water level can continue even as snow surface temperatures cool and meltwater generation ceases because it takes weeks to months for temperatures in the upper 10 m to decrease below 0°C. Drainage can last longer than the initial breakthrough time for surface melt to reach the aquifer (<2 days) because the mean travel time through the unsaturated zone is greater than the breakthrough time. The hydraulic conductivity decreases with decreasing moisture content, which further reduces flow through the unsaturated zone.

Once meltwater has entered the saturated zone, it flows horizontally and generally downhill, according to the hydraulic gradient, to discharge zones (likely at crevasses between the aquifer and the edge of the ice sheet, Miller et al., 2018). The hydraulic conductivity of the aquifer is 2.7×10^{-4} m/s (geometric standard deviation of 1.4), similar to an unconsolidated sand or gravel aquifer (Miller et al., 2017). The aquifer water comes to isotopic equilibrium with the surrounding firn with respect to tritium in the saturated zone. Discharge may occur into crevasses near the edge of the ice sheet and liquid filling these fracture zones may hydrofracture crevasses to the base of the ice sheet (McNerney, 2016; Poinar et al., 2017).

The temperature distribution within the ice sheet defines the bottom of the aquifer. The base occurs at the depth where the heat from the surface is inadequate to warm the ice to 0°C. Below this depth, subzero temperatures prevent liquid water from existing. Some refreezing occurs at the base of the aquifer, producing clear ice (no air bubbles) (Miller et al., 2018).

The firn aquifer alters the thermal regime of the ice sheet. The aquifer prevents cooling of the firn within the saturated zone to the mean annual air temperature (−11.3°C for 2016) and effectively separates the firn above the aquifer base from that below. Once the aquifer exists, the ice sheet thermal surface boundary condition effectively becomes the base of the aquifer instead of the snow surface because temperature variations above the aquifer base are buffered by the aquifer. The surface thermal boundary condition can be considered a constant temperature of 0°C instead of the mean annual air temperature in areas where firn aquifers exist. At such locations, this is a substantial alteration of the shallow temperature profile of the ice sheet and

may have important implications for ice sheet models, as well as historical records of environmental conditions and their preservation in ice cores.

The elevated specific conductance of aquifer water relative to snow indicates that the aquifer concentrates dissolved solids. The concentration of solutes in the aquifer is controlled by the amount of solutes within snow, the flux of meltwater through snow and the aquifer, and the rate of refreezing along the base of the aquifer. Modeling this process using parameter values constrained by field measurements suggests a mean residence time (e-folding time) of 6.5 years. These modeled values are within the range of measured values for SC, and the mean residence time is similar to estimates of the mean residence time (~8 to 23 years) derived from a water budget of the aquifer (Miller et al., 2018).

Increasing recharge through warmer surface temperatures, or increasing hydraulic conductivity by melting ice within the aquifer or developing fracture networks, will increase flow through the firn. Expansion of areas of high melt rates allows the aquifer to grow upslope as well. The aquifer formed between 1963 and 2006 and has expanded upslope since 2010.

5. Conclusions

This work describes cryohydrologic and geochemical field data collected in a perennial firn aquifer located in southeast Greenland, upslope from Helheim Glacier. The interpretation of these data are synthesized into a quantitative overview of the firn aquifer hydrology that supports numerical modeling and is likely applicable to firn aquifers in other regions. To date, this is now the most intensively studied firn aquifer in the world.

Beyond this description of the firn aquifer hydrology, much remains unknown about the effect meltwater has on firn metamorphism and implications for meltwater retention. Further investigation of tritium in precipitation at this site would aid firn dating. Additionally, further research is needed to develop an understanding of the impacts discharging firn-aquifer water may have on ice dynamics and sea level rise, and continued monitoring is needed to evaluate the apparent recent expansion of these aquifers.

Annually draining firn aquifers have been detected in mountain glaciers in the Cascade Mountains and the Alps (Fountain & Walder, 1998; Oerter & Moser, 1982) and a perennial aquifer has been identified in an arctic ice field (Christianson et al., 2015). While this study focuses on a much larger perennial firn aquifer in southeast Greenland, the general conceptual model can be applied to other firn aquifers in other regions, which are expected to become more important components of cryohydrologic systems as both the climate warms and scientific exploration advances. Further, as firn aquifers are a relatively new facies of ice sheet hydrology in the Arctic, and potentially Antarctic (Bell et al., 2018), a detailed description of their existence and function is required prior to extrapolating to other sites. Such description is also useful in contrasting meltwater movement and retention in firn aquifers to meltwater movement and retention in other settings where meltwater becomes runoff or refreezes in the firn column, such as surface streams and lakes, englacial lakes, or ice layers or ice slabs (Charalampidis et al., 2016; Cox et al., 2015; Harper et al., 2012; Lenaerts et al., 2016; MacFerrin et al., 2019; Machguth et al., 2016; Pfeffer et al., 1991; Smith et al., 2017). Application of methods applied at this firn aquifer to other sites will lead to deeper understanding of firn aquifers (which undoubtedly vary from this model at other locations) and the impact firn aquifers have on global glacier and ice sheet mass balance, runoff, and sea level rise.

Airborne radar data show that the aquifer above Helheim Glacier has in fact expanded upslope over time, presumably as melt area has expanded as a result, in part, of global climate change and the associated warming of the Arctic (Fettweis et al., 2011; Hanna et al., 2008). As surface melt increases under a warming climate, the aquifer will likely continue to expand upslope, leading to further alteration of the thermal regime of the ice sheet, while increased discharge could impact sea level rise and the rates of glacier movement through basal slip. As firn aquifer extent expands with increasing melt area and rates, more liquid water may move through firn aquifers. Increased discharge from draining aquifers may influence subglacial hydrology and ice flow (Poinar et al., 2019, 2017). The increased flux of liquid water transmitted through aquifers that ultimately drain to the ocean could increase the contribution of firn aquifers to sea level rise.

Data Availability Statement

Data can be found at the NSF Arctic Data Center. Specifically, hydrology data are available at this site (https://arcticdata.io/catalog/view/doi:10.18739/A26T0GW4P). Firn density data are available in the SUMup data set (https://arcticdata.io/catalog/view/doi:10.18739/A26D5PB2S). Weather station data can be found at this site (https://arcticdata.io/catalog/view/doi:10.18739/A26D5PB4R). Tritium, CFC, fluorescein dye, and firn stratigraphy data can be found at this site (https://arcticdata.io/catalog/view/doi:10.18739/A2F18SF5B). Firn salt data can be found at this site (https://arcticdata.io/catalog/view/doi:10.18739/A2NS0KZ0K). The firn temperatures and water level data can be found at https://arcticdata.io/catalog/view/doi:10.18739/A2R785P5W

References

Ambach, W., Blumthaler, M., & Kirchlechner, P. (1981). Application of the Gravity Flow Theory to the Percolation of Melt Water Through Firn. *Journal of Glaciology*, *27*(95), 67–75. https://doi.org/10.3189/S0022143000011230

Andreas, E. L. (1987). A theory for the scalar roughness and the scalar transfer coefficients over snow and sea ice. *Boundary-Layer Meteorology*, *38*(1–2), 159–184. https://doi.org/10.1007/BF00121562

Bales, R. C., Davis, R. E., & Williams, M. W. (1993). Tracer release in melting snow: Diurnal and seasonal patterns. *Hydrological Processes*, *7*(4), 389–401. https://doi.org/10.1002/hyp.3360070405

Bari, S. A., & Hallett, J. (1974). Nucleation and growth of bubbles at an ice–water interface. *Journal of Glaciology*, *13*(69), 489–520. https://doi.org/10.1017/S0022143000023248

Bell, R. E., Banwell, A. F., Trusel, L. D., & Kingslake, J. (2018). Antarctic surface hydrology and impacts on ice-sheet mass balance. *Nature Climate Change*, *8*(12), 1044–1052. https://doi.org/10.1038/s41558-018-0326-3

Braithwaite, R. J. (1985). Calculation of degree-days for glacier-climate research. *Zeitschrift Fue Gletscherkunde Und Glazialgeologie*, *20*, 1–8.

Charalampidis, C., Van As, D., Colgan, W. T., Fausto, R. S., Macferrin, M., & Machguth, H. (2016). Thermal tracing of retained meltwater in the lower accumulation area of the southwestern Greenland ice sheet. *Annals of Glaciology*, *57*(72), 1–10. https://doi.org/10.1017/aog.2016.2

Christianson, K., Kohler, J., Alley, R. B., Nuth, C., & van Pelt, W. J. J. (2015). Dynamic perennial firn aquifer on an Arctic glacier. *Geophysical Research Letters*, *42*, 1418–1426. https://doi.org/10.1002/2014GL062806

Chu, W., Schroeder, D. M., & Siegfried, M. R. (2018). Retrieval of englacial firn aquifer thickness from ice-penetrating radar sounding in southeastern Greenland. *Geophysical Research Letters*, *45*, 11,770–11,778. https://doi.org/10.1029/2018GL079751

Cook, P. G., & Solomon, D. K. (1997). Recent advances in dating young groundwater: Chlorofluorocarbons, $^3H^3He$ and ^{85}Kr. *Journal of Hydrology*, *191*(1-4), 245–265. https://doi.org/10.1016/S0022-1694(96)03051-X

Cox, C., Humphrey, N., & Harper, J. (2015). Quantifying meltwater refreezing along a transect of sites on the Greenland ice sheet. *The Cryosphere*, *9*(2), 691–701. https://doi.org/10.5194/tc-9-691-2015

CReSIS (2017). *Accumulation Radar and Radar Depth Sounder Data*. Lawrence, Kansas, USA: Digital Media. https://data.cresis.ku.edu/

DeWalle, D. R., & Rango, A. (2008). *Principles of snow hydrology*. Cambridge: Cambridge University Press. https://doi.org/10.1017/CBO9780511535673

Elkins, J. W., Thompson, T. M., Swanson, T. H., Butler, J. H., Hall, B. D., Cummings, S. O., et al. (1993). Decrease in the growth rates of atmospheric chlorofluorocarbons 11 and 12. *Nature*, *364*(6440), 780–783. https://doi.org/10.1038/364780a0

Enderlin, E. M., Howat, I. M., Jeong, S., Noh, M.-J., van Angelen, J. H., & van den Broeke, M. R. (2014). An improved mass budget for the Greenland ice sheet. *Geophysical Research Letters*, *41*(3), 866–872. https://doi.org/10.1002/2013GL059010

Fettweis, X., Tedesco, M., Van Den Broeke, M., & Ettema, J. (2011). Melting trends over the Greenland ice sheet (1958–2009) from spaceborne microwave data and regional climate models. *The Cryosphere*, *5*(2), 359–375. https://doi.org/10.5194/tc-5-359-2011

Forster, R. R., Box, J. E., van den Broeke, M. R., Miège, C., Burgess, E. W., van Angelen, J. H., et al. (2014). Extensive liquid meltwater storage in firn within the Greenland ice sheet. *Nature Geoscience*, *7*(2), 95–98. https://doi.org/10.1038/ngeo2043

Fountain, A. G. (1989). The storage of water in, and hydraulic characteristics of, the firn of South Cascade glacier, Washington state, USA. *Annals of Glaciology*, *13*, 69–75. https://doi.org/10.1017/S0260305500007667

Fountain, A. G., & Walder, J. S. (1998). Water flow through temperate glaciers. *Reviews of Geophysics*, *36*(3), 299–328. https://doi.org/10.1029/97RG03579

Fourré, E., Jean-Baptiste, P., Dapoigny, A., Baumier, D., Petit, J., & Jouzel, J. (2006). Past and recent tritium levels in Arctic and Antarctic polar caps. *Earth and Planetary Science Letters*, *245*(1–2), 56–64. https://doi.org/10.1016/j.epsl.2006.03.003

Garber, M. S., & Koopman, F. C. (1968). Methods of measuring water levels in deep wells. In *U.S. Geological Survey Techniques of Water-Resources Investigations* (p. 23). https://pubs.usgs.gov/twri/twri8a1/

Hanna, E., Huybrechts, P., Steffen, K., Cappelen, J., Huff, R., Shuman, C., et al. (2008). Increased runoff from melt from the Greenland ice sheet: A response to global warming. *Journal of Climate*, *21*(2), 331–341. https://doi.org/10.1175/2007JCLI1964.1

Harper, J., Humphrey, N., Pfeffer, W. T., Brown, J., & Fettweis, X. (2012). Greenland ice-sheet contribution to sea-level rise buffered by meltwater storage in firn. *Nature*, *491*(7423), 240–243. https://doi.org/10.1038/nature11566

Healy, R. W. (2010). Water-budget methods. In Estimating groundwater recharge (pp. 15–42). Retrieved from https://doi.org/10.1017/CBO9780511780745.003

Helm, V., Humbert, A., & Miller, H. (2014). Elevation and elevation change of Greenland and Antarctica derived from CryoSat-2. *The Cryosphere*, *8*(4), 1539–1559. https://doi.org/10.5194/tc-8-1539-2014

Hock, R. (2003). Temperature index melt modelling in mountain areas. *Journal of Hydrology*, *282*(1-4), 104–115. https://doi.org/10.1016/S0022-1694(03)00257-9

Humphrey, N. F., Harper, J. T., & Pfeffer, W. T. (2012). Thermal tracking of meltwater retention in Greenland's accumulation area. *Journal of Geophysical Research*, *117*, F01010. https://doi.org/10.1029/2011JF002083

Kawashima, K. (1997). Formation processes of ice body revealed by the internal structure of perennial snow patches in Japan. *Bulletin of Glacier Research*, *15*, 1–10.

Koenig, L., Miège, C., Forster, R. R., & Brucker, L. (2014). Initial in situ measurements of perennial meltwater storage in the Greenland firn aquifer. *Geophysical Research Letters*, *41*, 81–85. https://doi.org/10.1002/2013GL058083

Koenig, L., & Montgomery, L. (2019). Surface mass balance and snow depth on sea ice working group (SUMup) snow density subdataset, Greenland and Antartica, 1950–2018. Arctic Data Center. https://doi.org/10.18739/A26D5PB2S

Koerner, R. M. (1997). Some comments on climatic reconstructions from ice cores drilled in areas of high melt. *Journal of Glaciology*, *43*(143), 90–97. https://doi.org/10.3189/S0022143000002847

Koide, M., Michel, R., Goldberg, E. D., Herron, M. M., & Langway, C. C. (1982). Characterization of radioactive fallout from pre- and post-moratorium tests to polar ice caps. *Nature*, *296*(5857), 544–547. https://doi.org/10.1038/296544a0

Studinger, M. (2020). *IceBridge ATM L2 Icessn Elevation, Slope, and Roughness, Version 2. [2010 - 2017]*. Boulder, CO, USA: NASA National Snow and Ice Data Center Distributed Active Archive Center. https://doi.org/10.5067/CPRXXK3F39RV

Kuipers Munneke, P., Ligtenberg, M., van den Broeke, M. R., van Angelen, J. H., & Forster, R. R. (2014). Explaining the presence of perennial liquid water bodies in the firn of the Greenland ice sheet. *Geophysical Research Letters*, *41*, 476–483. https://doi.org/10.1002/2013GL058389

Kuipers Munneke, P., Smeets, C. J. P. P., Reijmer, C. H., Oerlemans, J., van de Wal, R. S. W., & van den Broeke, M. R. (2018). The K-transect on the western Greenland ice sheet: Surface energy balance (2003–2016). *Arctic, Antarctic, and Alpine Research*, *50*(1), 1–13. https://doi.org/10.1080/15230430.2017.1420952

Legchenko, A., Miège, C., Koenig, L. S., Forster, R. R., Miller, O., Solomon, D. K., et al. (2018a). Estimating water volume stored in the South-Eastern Greenland firn aquifer using magnetic-resonance soundings. *Journal of Applied Geophysics*, *150*, 11–20. https://doi.org/10.1016/j.jappgeo.2018.01.005

Legchenko, A., Miège, C., Koenig, L. S., Forster, R. R., Miller, O., Solomon, D. K., et al. (2018b). Investigating a firn aquifer near Helheim Glacier (South-Eastern Greenland) with magnetic resonance soundings and ground-penetrating radar. *Near Surface Geophysics*, *16*(4), 411–422. https://doi.org/10.1002/nsg.12001

Lenaerts, J. T. M., Lhermitte, S., Drews, R., Ligtenberg, S. R. M., Berger, S., Helm, V., et al. (2016). Meltwater produced by wind–albedo interaction stored in an East Antarctic ice shelf. *Nature Climate Change*, *7*(1), 58–62. https://doi.org/10.1038/nclimate3180

Lewis, C., Gogineni, S., Rodriguez-Morales, F., Panzer, B., Stumpf, T., Paden, J., & Leuschen, C. (2015). Airborne fine-resolution UHF radar: An approach to the study of englacial reflections, firn compaction and ice attenuation rates. *Journal of Glaciology*, *61*(225), 89–100. https://doi.org/10.3189/2015JoG14J089

Lovely, A., Loose, B., Schlosser, P., McGillis, W., Zappa, C., Perovich, D., et al. (2015). The gas transfer through Polar Sea ice experiment: Insights into the rates and pathways that determine geochemical fluxes. *Journal of Geophysical Research: Oceans*, *120*, 8177–8194. https://doi.org/10.1002/2014JC010607

Lucas, L. L., & Unterweger, M. P. (2000). Comprehensive Review and Critical Evaluation of the Half-Life of Tritium. *Journal of Research of the National Institute of Standards and Technology*, *105*(4), 541–549. https://doi.org/10.6028/jres.105.043

MacFerrin, M., Machguth, H., van As, D., Charalampidis, C., Stevens, C. M., Heilig, A., et al. (2019). Rapid expansion of Greenland's low-permeability ice slabs. *Nature*, *573*(7774), 403–407. https://doi.org/10.1038/s41586-019-1550-3

MacFerrin, M. J. (2018). Rapid expansion of Greenland's low-permeability ice slabs in a warming climate. Cooperative Institute for Research in Environmental Sciences Graduate Theses & Dissertations. Retrieved from https://scholar.colorado.edu/cires_gradetds/1

Machguth, H., MacFerrin, M., van As, D., Box, J. E., Charalampidis, C., Colgan, W., et al. (2016). Greenland meltwater storage in firn limited by near-surface ice formation. *Nature Climate Change*, *6*(4), 390–393. https://doi.org/10.1038/nclimate2899

McConnell, J. (2020). Chemical measurements in the Arctic Circle Traverse 2011 (ACT11) ice cores. Arctic Data Center. https://doi.org/10.18739/A2NS0KZ0K

McConnell, J. R., Burke, A., Dunbar, N. W., Köhler, P., Thomas, J. L., Arienzo, M. M., et al. (2017). Synchronous volcanic eruptions and abrupt climate change ~17.7 ka plausibly linked by stratospheric ozone depletion. *Proceedings of the National Academy of Sciences*, *114*(38), 10,035–10,040. https://doi.org/10.1073/pnas.1705595114

McConnell, J. R., & Edwards, R. (2008). Coal burning leaves toxic heavy metal legacy in the Arctic. *Proceedings of the National Academy of Sciences*, *105*(34), 12,140–12,144. https://doi.org/10.1073/pnas.0803564105

McConnell, J. R., Lamorey, G. W., Lambert, S. W., & Taylor, K. C. (2002). Continuous ice-core chemical analyses using inductively coupled plasma mass spectrometry. *Environmental Science & Technology*, *36*(1), 7–11. https://doi.org/10.1021/es011088z

McNerney, L. (2016). Constraining the Greenland firn aquifer's ability to hydrofracture a crevasse to the bed of the ice sheet. University of Utah, thesis. Retrieved from https://collections.lib.utah.edu/details?id=197636

Miège, C., Forster, R. R., Box, J. E., Burgess, E. W., Mcconnell, J. R., Pasteris, D. R., & Spikes, V. B. (2013). Southeast Greenland high accumulation rates derived from firn cores and ground-penetrating radar. *Annals of Glaciology*, *54*(63), 322–332. https://doi.org/10.3189/2013AoG63A358

Miège, C., Forster, R., Brucker, L., Koenig, L., Miller, O., Solomon, K., & Schmerr, N. (2020). Firn temperatures (2013–2017) and water-level changes (2015–2017) collected at three locations in a firn-aquifer region of the southeastern part of the Greenland Ice Sheet. Arctic Data Center. https://doi.org/10.18739/A2R785P5W

Miège, C., Forster, R. R., Brucker, L., Koenig, L. S., Solomon, D. K., Paden, J. D., et al. (2016). Spatial extent and temporal variability of Greenland firn aquifers detected by ground and airborne radars. *Journal of Geophysical Research: Earth Surface*, *121*, 2381–2398. https://doi.org/10.1002/2016JF003869

Miller, O., Solomon, D. K., Miège, C., Koenig, L., Forster, R., Schmerr, N., et al. (2018). Direct evidence of meltwater flow within a firn aquifer in Southeast Greenland. *Geophysical Research Letters*, *45*, 207–215. https://doi.org/10.1002/2017GL075707

Miller, O., & Solomon, K. (2019). Hydrologic data from a firn aquifer in Southeast Greenland, 2015–2016. Arctic Data Center. https://doi.org/10.18739/A26T0GW4P

Miller, O., Solomon, L., Miège, CL., Forster, R., & Koenig, L. (2019). Physical and chemical data from a firn aquifer in Southeast Greenland, 2015–2016. Arctic Data Center. https://doi.org/10.18739/A2F18SF5B

Miller, O. L., Solomon, D. K., Miège, C., Koenig, L. S., Forster, R. R., Montgomery, L. N., et al. (2017). Hydraulic conductivity of a firn aquifer in Southeast Greenland. *Frontiers in Earth Science*, *5*, 38. https://doi.org/10.3389/feart.2017.00038

Montgomery, L. N., Schmerr, N., Burdick, S., Forster, R. R., Koenig, L., Legchenko, A., et al. (2017). Investigation of firn aquifer structure in southeastern Greenland using active source seismology. *Frontiers in Earth Science*, *5*, 10. https://doi.org/10.3389/feart.2017.00010

National Oceanic and Atmospheric Administration (n.d.). Earth system research laboratory global monitoring division. Retrieved from https://www.esrl.noaa.gov/gmd/dv/

Oerter, H., & Moser, H. (1982). Water storage and drainage within the firn of a temperate glacier (Vernagtferner, Oetztal Alps, Austria). In J. W. Glen (Ed.), *Hydrological aspects of alpine and high mountain areas (proceedings of the Exeter symposium)* (Vol. 138, pp. 71–81). Exeter: IAHS Publ.

Oyabu, I., Matoba, S., Yamasaki, T., Kadota, M., & Iizuka, Y. (2016). Seasonal variations in the major chemical species of snow at the south east dome in Greenland. *Polar Science*, *10*(1), 36–42. https://doi.org/10.1016/j.polar.2016.01.003

Pfeffer, W. T., Meier, M. F., & Illangasekare, T. H. (1991). Retention of Greenland runoff by refreezing: Implications for projected future sea level change. *Journal of Geophysical Research*, *96*(C12), 22117. https://doi.org/10.1029/91JC02502

Poinar, K., Dow, C. F., & Andrews, L. C. (2019). Long-term support of an active subglacial hydrologic system in Southeast Greenland by firn aquifers. *Geophysical Research Letters*, *46*, 4772–4781. https://doi.org/10.1029/2019GL082786

Poinar, K., Joughin, I., Lilien, D., Brucker, L., Kehrl, L., & Nowicki, S. (2017). Drainage of Southeast Greenland firn aquifer water through crevasses to the bed. *Frontiers in Earth Science*, *5*, 5. https://doi.org/10.3389/FEART.2017.00005

Reijmer, C., Kuipers Munneke, P., & Smeets, P. (2019). Helhein firn aquifer weather station data and melt rates, Greenland, 2014–2016. Arctic Data Center. https://doi.org/10.18739/A26D5PB4R

Risser, D. W., Gburek, W. J., & Folmar, G. J. (2005). Comparison of methods for estimating ground-water recharge and base flow at a small watershed underlain by fractured bedrock in the eastern United States. In *U.S. Geological Survey Scientific Investigations Report 2005–5038* (p. 31). https://doi.org/10.3133/sir20055038

Rodriguez-Morales, F., Gogineni, S., Leuschen, C. J., Paden, J. D., Li, J., Lewis, C. C., et al. (2014). Advanced multifrequency radar instrumentation for polar research. *IEEE Transactions on Geoscience and Remote Sensing*, *52*(5), 2824–2842. https://doi.org/10.1109/TGRS.2013.2266415

Schneider, T. (1999). Water movement in the firn of Storglaciaren, Sweden. *Journal of Glaciology*, *45*(150), 286–294. https://doi.org/10.3189/002214399793377211

Schneider, T., & Jansson, P. (2004). Internal accumulation in firn and its significance for the mass balance of Storglaciären, Sweden. *Journal of Glaciology*, *50*(168), 25–34. https://doi.org/10.3189/172756504781830277

Sharp, R. P. (1951). Features of the firn on upper Seward glacier St. Elias Mountains, Canada. *The Journal of Geology*, *59*(6), 599–621. https://doi.org/10.1086/625915

Sigl, M., Fudge, T. J., Winstrup, M., Cole-Dai, J., Ferris, D., McConnell, J. R., et al. (2016). The WAIS divide deep ice core WD2014 chronology—Part 2: Annual-layer counting (0–31 ka BP). *Climate of the Past*, *12*(3), 769–786. https://doi.org/10.5194/cp-12-769-2016

Smith, L. C., Yang, K., Pitcher, L. H., Overstreet, B. T., Chu, V. W., Rennermalm, Å. K., et al. (2017). Direct measurements of meltwater runoff on the Greenland ice sheet surface. *Proceedings of the National Academy of Sciences*, *114*(50), E10622–E10631. https://doi.org/10.1073/pnas.1707743114

Steger, C. R., Reijmer, C. H., van den Broeke, M. R., Wever, N., Forster, R. R., Koenig, L. S., et al. (2017). Firn meltwater retention on the Greenland ice sheet: A model comparison. *Frontiers in Earth Science*, *5*, 3. https://doi.org/10.3389/feart.2017.00003

Tóth, J. (1963). A theoretical analysis of groundwater flow in small drainage basins. *Journal of Geophysical Research*, *68*(16), 4795–4812. https://doi.org/10.1029/JZ068i016p04795

Vallon, M., Petit, J.-R., & Fabre, B. (1976). Study of an ice core to the bedrock in the accumulation zone of an alpine glacier. *Journal of Glaciology*, *17*(75), 13–28. https://doi.org/10.1017/S0022143000030677

van Angelen, J. H., Lenaerts, J. T. M., Lhermitte, S., Fettweis, X., Kuipers Munneke, P., van den Broeke, M. R., et al. (2012). Sensitivity of Greenland ice sheet surface mass balance to surface albedo parameterization: A study with a regional climate model. *The Cryosphere*, *6*(5), 1175–1186. https://doi.org/10.5194/tc-6-1175-2012

van Angelen, J. H., Lenaerts, M., van den Broeke, M. R., Fettweis, X., & van Meijgaard, E. (2013). Rapid loss of firn pore space accelerates 21st century Greenland mass loss. *Geophysical Research Letters*, *40*, 2109–2113. https://doi.org/10.1002/grl.50490

van den Broeke, M., Bus, C., Ettema, J., & Smeets, P. (2010). Temperature thresholds for degree-day modelling of Greenland ice sheet melt rates. *Geophysical Research Letters*, *37*, L18501. https://doi.org/10.1029/2010GL044123

van der Wel, L. G., Streurman, H. J., Isaksson, E., Helsen, M. M., van de Wal, R. S. W., Martma, T., et al. (2011). Using high-resolution tritium profiles to quantify the effects of melt on two Spitsbergen ice cores. *Journal of Glaciology*, *57*(206), 1087–1097. https://doi.org/10.3189/002214311798843368

Yang, Q., Mayewski, P. A., Linder, E., Whitlow, S., & Twickler, M. (1996). Chemical species spatial distribution and relationship to elevation and snow accumulation rate over the Greenland ice sheet. *Journal of Geophysical Research*, *101*(D13), 18,629–18,637. https://doi.org/10.1029/96JD01061